



1 **WRF-Chem simulated surface ozone over South Asia during**
2 **the pre-monsoon: Effects of emission inventories and chemical**
3 **mechanisms**

4 **Amit Sharma^{1,2,*}, Narendra Ojha^{2,*}, Andrea Pozzer², Kathleen A. Mar³, Gufran Beig⁴,**
5 **Jos Lelieveld^{2,5}, and Sachin S. Gunthe¹**

6 ¹Department of Civil Engineering, Indian Institute of Technology Madras, Chennai, India

7 ²Atmospheric Chemistry Department, Max Planck Institute for Chemistry, Mainz, Germany

8 ³Institute for Advanced Sustainability Studies, Potsdam, Germany

9 ⁴Indian Institute for Tropical Meteorology, Pune, India

10 ⁵Energy, Environment and Water Research Center, The Cyprus Institute, Nicosia, Cyprus

11
12 *Correspondence to: Amit Sharma (amit.iit87@gmail.com) and Narendra Ojha (narendra.ojha@mpic.de)

13
14
15 **Abstract**

16 We evaluate numerical simulations of surface ozone mixing ratios over the South Asian region during the pre-
17 monsoon season employing three different emission inventories (EDGAR-HTAP, INTEX-B, and SEAC4RS) in
18 the WRF-Chem model with the RADM2 chemical mechanism. Evaluation of modelled ozone and its diurnal
19 variability, using data from a network of 18 monitoring stations across South Asia, show the model ability to
20 reproduce the clean, rural and polluted urban environments over this region. In contrast to the diurnal average, the
21 modelled ozone mixing ratios during the noontime i.e. hours of intense photochemistry (1130-1630 h Indian
22 Standard Time or IST) are found to differ among the three inventories. This suggests that evaluations of the
23 modelled ozone limited to 24-h average are insufficient to comprehend the uncertainties associated with ozone
24 build-up. HTAP generally shows 10-30 ppbv higher noontime ozone mixing ratios than SEAC4RS and INTEX-B,
25 especially over the north-west Indo-Gangetic Plain (IGP), central India and southern India. Further, the model
26 performance shows strong spatial heterogeneity, with SEAC4RS leading to better agreement with observations
27 over east and south India, whereas HTAP performs better over north and central India, and INTEX-B over west
28 India. The Normalized Mean Bias (NMB in %) in the noontime ozone over the entire South Asia is found to be
29 lowest for the SEAC4RS (~11%), followed by INTEX-B (~12.5%) and HTAP (~22%). The HTAP simulation
30 repeated with the alternative MOZART chemical mechanism showed even more strongly enhanced surface ozone
31 mixing ratios (noontime NMB=36.5%) due to vertical mixing of enhanced ozone that has been produced aloft. The
32 SEAC4RS inventory with the RADM2 chemical mechanism is found to be the most successful overall among the
33 configurations evaluated here in simulating ozone air quality over South Asia. Our study indicates the need to also
34 evaluate the O₃ precursors across a network of stations to further reduce uncertainties in modelled ozone.

35
36
37
38



39 1. Introduction

40 Tropospheric ozone plays central roles in atmospheric chemistry, air quality and climate change. Unlike primary
41 pollutants, which are emitted directly, tropospheric ozone forms photochemically involving precursors such as
42 carbon monoxide (CO), volatile organic compounds (VOCs) and oxides of nitrogen (NO_x), supplemented by
43 transport from the stratosphere (e.g. Crutzen, 1974; Atkinson, 2000; Monks et al., 2015). It can be transported over
44 long distances resulting in enhanced concentrations even in areas located remote from the sources of precursors
45 (Cox et al., 1975). The photochemical production of ozone and its impacts on agricultural crops and human health
46 are especially pronounced near the surface. Numerous studies have shown that elevated surface ozone levels
47 significantly reduce crop yields (e. g.; Krupa et al., 1998; Emberson et al., 2009; Ainsworth et al., 2012; Wilkinson
48 et al., 2012), in addition to adverse human health effects that cause premature mortality (e.g., Bell et al., 2004;
49 Jerrett et al., 2009; Anenberg et al., 2010; Lelieveld et al., 2015).

50 An accurate representation of anthropogenic emissions of ozone precursors is essential to understand the
51 photochemical production of ozone and support policy making. While anthropogenic emissions have been nearly
52 stable or decreasing over northern America and Europe (e. g. Yoon and Pozzer, 2014), there has been substantial
53 enhancement over the East and South Asian regions in recent decades (e. g. Akimoto, 2003; Ohara et al., 2007,
54 Logan et al., 2012; Gurjar et al., 2016). The number of premature mortalities per year due to outdoor air pollution
55 is anticipated to double by the year 2050 as compared to the year 2010 in a business-as-usual scenario,
56 predominantly in Asia (Lelieveld et al., 2015). The multi-pollutant index over all populated regions in the northern
57 hemisphere shows a general increase, with South Asia being the major hotspot of deteriorating air quality (Pozzer
58 et al., 2012).

59 The growth of anthropogenic emissions over the South Asian region has regional implications, and is also
60 predicted to influence air quality on a hemispheric scale (Lelieveld and Dentener, 2000). It was shown that the
61 anthropogenic emissions and their subsequent photochemical degradation over South Asia influence air quality
62 over the Himalayas (e.g. Ojha et al., 2012; Sarangi et al., 2014) and the Tibetan Plateau (Lüthi et al., 2015) as well
63 as the marine environment downwind of India (e.g. Lawrence and Lelieveld, 2010). Additionally, the prevailing
64 synoptic scale weather patterns make this region highly conducive to long-range export of pollutants (e.g.
65 Lelieveld et al., 2002; Lawrence et al., 2003; Ojha et al., 2014; Zanis et al., 2014). Therefore, the accurate
66 estimation of anthropogenic emissions over South Asia and their representation in chemical transport models are
67 essential to quantify the effects on regional as well as global air quality.

68 The Weather Research and Forecasting model with Chemistry (WRF-Chem) (Grell et al., 2005; Fast et al., 2006),
69 a regional simulation system, has been popular for use over the South Asian region in numerous recent studies to
70 simulate the meteorology and spatio-temporal distribution of ozone and related trace gases (e. g. Kumar et al.,
71 2012a, 2012b; Michael et al., 2013; Gupta et al., 2015; Jena et al., 2015; Ansari et al., 2016; Ojha et al., 2016;
72 Girach et al., 2016). WRF-Chem simulations at higher spatial resolution employing regional emission inventories
73 have been shown to better reproduce the observed spatial and temporal heterogeneities in ozone over this region as
74 compared to the global models (e.g. Kumar et al., 2012b; Ojha et al., 2016). However, an evaluation of modelled
75 ozone based on data from a network of stations across South Asia is imperative considering very large spatio-
76 temporal heterogeneity in the distribution of ozone over this region (e.g. Kumar et al., 2010; Ojha et al., 2012;
77 Kumar et al., 2012b) mainly resulting from heterogeneous precursor sources. WRF-Chem simulated ozone



78 distributions have also been utilized to assess the losses in crop yields, and it was suggested that the estimated crop
79 losses would be sufficient to feed about 94 million people living below the poverty line in this region (Ghude et
80 al., 2014). Further, WRF-Chem has been used to estimate that premature mortality in India caused by chronic
81 obstructive pulmonary disease (COPD) due to surface O₃ exposure was ~12,000 people in the year 2011 (Ghude et
82 al., 2016). Despite these applications, there is room for improvement in modeled concentrations as some limited
83 studies evaluating ozone on diurnal scales revealed a significant overestimation of noontime ozone e.g. by as much
84 as 20 ppbv in Kanpur (Michael et al., 2013) and 30 ppbv in Delhi (Gupta and Mohan, 2015).

85 Using WRF-Chem, Amnuaylojaroen et al. (2014) showed that over continental southeast Asia surface ozone
86 mixing ratios vary little (~4.5%) among simulations employing different emission inventories. A recent study by
87 Mar et al. (2016) highlighted the dependence of WRF-Chem predicted ozone air quality (over Europe) on the
88 chosen chemical mechanism. These results indicate the need for evaluating the effects of emission inventories and
89 chemical mechanisms on the model performance using a network of stations across South Asia, which has not
90 been carried out thus far. The main objectives of the present study are:

- 91 (a) To evaluate WRF-Chem simulated ozone over South Asia, including the diurnal cycle, against recent in situ
92 measurements from a network of stations;
- 93 (b) To inter-compare model simulated O₃ among different emission inventories;
- 94 (c) To inter-compare model simulated O₃ between two extensively used chemical mechanisms (MOZART and
95 RADM2) with the same emission inventory;
- 96 (d) To provide recommendations on the model configuration for future studies over stations, sub-regions as well
97 as the entire South Asian region.

98
99 We focus on the pre-monsoon season (March-May) for the study as O₃ mixing ratios at the surface are generally
100 the highest over most of South Asia during this period (Jain et al., 2005; Debaje et al., 2006; Reddy et al., 2010;
101 Ojha et al., 2012; Gaur et al., 2014; Renuka et al., 2014; Bhuyan et al., 2014; Sarangi et al., 2014; Yadav et al.,
102 2014; Sarkar et al., 2015). This is because photochemistry over South Asia is most intense during this season
103 caused by the combined effects of high pollution loading, biomass-burning emissions and a lack of precipitation.
104 Section 2 presents the model description, including physics and chemistry options, emission inputs and the
105 observational data. Model evaluation focussing on the effects of different emission inventories on ozone is
106 presented in section 3. The inter-comparison between the RADM2 and MOZART chemical mechanism is
107 discussed in section 4. For the list of symbols and acronyms used in this paper are listed in Table 1. The sub-
108 regional and South Asian domain evaluation and recommendations on model configuration are provided in section
109 5, followed by the summary and conclusions drawn from the study in section 6.

110 2. Methodology

111 2.1. WRF-Chem

112 In this study we use the Weather Research and Forecasting model coupled with chemistry (WRF-Chem version
113 3.5.1), which is an online mesoscale model capable of simulating meteorological and chemical processes
114 simultaneously (Grell et al., 2005; Fast et al., 2006). The model domain (Fig. 1) is defined on a mercator
115 projection and is centred at 22° N, 83° E with 274 and 352 grid points in the east-west and north-south directions,
116 respectively, at the horizontal resolution of 12 km x 12 km. The land use data is incorporated from the US



117 Geological Survey (USGS) based on 24 land use categories. The ERA-interim reanalysis dataset from ECMWF
118 (<http://www.ecmwf.int/en/research/climate-reanalysis/browse-reanalysis-datasets>), archived at the horizontal
119 resolution of about 0.7° and temporal resolution of 6 hours, is used to provide the initial and lateral boundary
120 conditions for the meteorological calculations. All simulations in the study have been conducted for the period:
121 26th February – 31st May, 2013 at a time step of 72 s. The model output is stored every hour for analysis. The first
122 three days of model output have been discarded as model spin up.

123 Radiative transfer in the model has been represented using the Rapid Radiative Transfer Model (RRTM) longwave
124 scheme (Mlawer, 1997) and the Goddard shortwave scheme (Chou and Suarez, 1994). Surface physics is
125 parameterized using the Unified Noah land surface model (Tewari et al., 2004) along with eta similarity option
126 (Monin and Obukhov, 1954; Janjic, 1994, 1996), and the planetary boundary layer (PBL) is based on the Mellor-
127 Yamada-Janjic (MYJ) scheme (Mellor and Yamada, 1982; Janjic, 2002). The cloud microphysics is represented
128 by the Lin et al. scheme (Lin et al., 1983), and cumulus convection is parameterized using the Grell 3D Ensemble
129 Scheme (Grell, 1993; Grell and Devenyi, 2002). Four-dimensional data assimilation (FDDA) is incorporated for
130 nudging to limit the drift in the model simulated meteorology from the ERA-interim reanalysis (Stauffer and
131 Seaman, 1990; Liu et al. 2008). Horizontal winds are nudged at all vertical levels, whereas temperature and water
132 vapour mixing ratios are nudged above the PBL (Stauffer et al. 1990, 1991). The nudging coefficients for
133 temperature and horizontal winds are set as $3 \times 10^{-4} \text{ s}^{-1}$ whereas it is set as 10^{-5} s^{-1} for water vapour mixing ratio
134 (Otte, 2008).

135 This study utilizes two different chemical mechanisms, the Regional Acid Deposition Model - 2nd generation
136 (RADM2) (Stockwell et al., 1990), and the Model for Ozone and Related Chemical Tracers-version 4 (MOZART-
137 4) (Emmons et al., 2010). RADM2 chemistry includes 63 chemical species participating in 136 gas phase and 21
138 photolysis reactions. MOZART chemistry includes 81 chemical species participating in 159 gas phase and 38
139 photolysis reactions. Aerosols are represented using the Modal Aerosol Dynamics Model for Europe/ Secondary
140 Organic Aerosol Model (MADE/ SORGAM) (Ackermann et al., 1998; Schell et al., 2001) with RADM2 and
141 Global Ozone Chemistry Aerosol Radiation and Transport (GOCART) (Chin et al., 2000) with MOZART. The
142 photolysis rates are calculated using Fast-J photolysis scheme (Wild et al., 2000) in RADM2 simulations and
143 Madronich F-TUV scheme in MOZART simulation. The Madronich F-TUV photolysis scheme uses
144 climatological O_3 and O_2 overhead columns. The treatment of dry deposition process also differs between RADM2
145 and MOZART owing to differences in Henry's Law coefficients and diffusion coefficients. The chemical initial
146 and lateral boundary conditions are provided from 6 hourly fields from the Model for Ozone and Related
147 Chemical Tracers (MOZART-4/GEOS5) (<http://www.acom.ucar.edu/wrf-chem/mozart.shtml>).

148 2.2. Emission inputs

149 This study utilizes three different inventories for the anthropogenic emissions: HTAP, INTEX-B and the
150 SEAC4RS, which are briefly described here. The Hemispheric Transport of Air Pollution (HTAP) inventory
151 (Janssens-Maenhout et al., 2015) for anthropogenic emissions (http://edgar.jrc.ec.europa.eu/htap_v2/index.php?SECURE=_123) available for the year 2010 has been used. The HTAP inventory has been developed
153 by complementing various regional emissions with EDGAR data, in which Asian region including India is
154 represented by the Model Intercomparison study for Asia (MICS-Asia) inventory, which is at a horizontal
155 resolution of $0.25^\circ \times 0.25^\circ$ (Carmichael et al., 2008). The resultant global inventory is re-gridded at the spatial



156 resolution of $0.1^\circ \times 0.1^\circ$ and temporal resolution of 1 month. HTAP includes emissions of CO, NO_x, SO₂,
157 NM VOCs, PM, BC and OC from power, industry, residential, agriculture, ground transport and shipping sectors.
158 The Intercontinental Chemical Transport Experiment-Phase B (INTEX-B) inventory (Zhang et al., 2009),
159 developed to support the INTEX-B field campaign by the National Aeronautics and Space Administration
160 (NASA) in spring 2006, is the second inventory used in this study. It provides total emissions for year 2006 at a
161 horizontal resolution of $0.5^\circ \times 0.5^\circ$. The emission sectors include power generation, industry, residential and
162 transportation. The Southeast Asia Composition, Cloud, Climate Coupling Regional Study (SEAC4RS) inventory
163 (Lu and Streets, 2012), prepared for the NASA SEAC4RS field campaign, is the third inventory used in this study.
164 It provides total emissions for the year 2012 at a spatial resolution of $0.1^\circ \times 0.1^\circ$. The SEAC4RS and INTEX-B did
165 not cover regions in the north western part of the domain, and therefore we complemented this region (longitude <
166 75°E and latitude > 25°N) by HTAP emission data. The emissions of CO, NM VOCs and NO_x emissions among
167 the three emission inventories, as included in the simulations, are shown in Fig. 2. Table 2 provides estimates of
168 total emissions over different regions (as defined in Fig.1) from the three inventories. The emissions from biomass
169 burning are included using the Fire Inventory from NCAR (FINN) version 1.0 (Wiedinmyer et al., 2011). Model
170 of Emissions of Gases and Aerosols from Nature (MEGAN) is used to include the biogenic emissions (Guenther et
171 al., 2006) in the model.

172 The HTAP inventory is available at monthly temporal resolution while INTEX-B and SEAC4RS are available as
173 annual averages; however, seasonal variability in anthropogenic emissions may not have a major effect in this
174 study as we focus here on spring (pre-monsoon), for which monthly emissions are similar to the annual mean
175 (seasonal factor close to unity) (Supplementary material - Fig. S1; also see Fig. 2b in Kumar et al., 2012b).
176 Nevertheless, seasonal influence during spring is strongest for biomass-burning emissions, which have been
177 accounted for. The emissions from all inventories were injected in the lowest model layer. The diurnal profiles of
178 the anthropogenic emissions of ozone precursors, specific to South Asia are not available. A sensitivity simulation
179 implementing the diurnal emission profile available for Europe (Mar et al., 2016 and references therein) showed a
180 little impact on predicted noontime ozone over South Asia (Supplementary material – Fig S2).

181 2.3. Simulations

182 We have conducted 4 different numerical simulations as summarized in Table 3 and briefly described here. Three
183 simulations correspond to three different emission inventories HTAP, INTEX-B and SEAC4RS for the
184 anthropogenic emissions of ozone precursors, employing the RADM2 chemical mechanism. These simulations are
185 named HTAP-RADM2, INTEX-RADM2 and S4RS-RADM2 respectively. The emissions of aerosols have been
186 kept same (HTAP) among these three simulations and aerosol-radiation feedback has been switched off to
187 specifically identify the effects of emissions of O₃ precursors on modelled ozone. An additional simulation HTAP-
188 MOZ has been conducted to investigate the sensitivity of ozone to the employed chemical mechanism (MOZART
189 vs RADM2) by keeping the emissions fixed to HTAP.

190 2.4. Observational dataset

191 Surface ozone data is acquired from various studies and sources, as given in Table 4. In general, surface O₃
192 measurements over these stations have been conducted using the well-known technique of UV light absorption by
193 ozone molecules at about 254 nm, making use of Beer-Lambert's Law. The accuracy of these measurements is
194 reported to be about 5% (Kleinmann et al., 1994). The response time of such instruments is about 20 s and



195 instruments have a lower detection limit of 1 ppbv (Ojha et al., 2012). Here we have used the hourly and monthly
196 average data for the model evaluation. The details of instruments and calibrations at individual stations can be
197 found in the references given in the Table 4.

198 As simultaneous measurements at different stations are very sparse over South Asia, the model evaluation has
199 often to be conducted using observations of the same season/month of a different year (e. g. Kumar et al., 2012b;
200 Kumar et al., 2015; Ojha et al., 2016). However, to minimize the effect of temporal differences we preferentially
201 used measurements of recent years i.e. the observations at ~83% of the stations used in this study are of the period:
202 2009-2013. For four stations: Delhi (north India), Jabalpur (central India), Pune (west India) and Thumba (south
203 India), the observations and simulations are for the same year (2013). The observations at three stations have been
204 collected in previous periods (2004 or before). Finally, we investigated the effects of temporal differences on the
205 results and model biases presented here by conducting another simulation for a different year (2010)
206 (Supplementary material, Fig. S3).

207 **3. Effects of emission inventories**

208 **3.1. Spatial distribution of Ozone**

209 The spatial distribution of WRF-Chem simulated 24-h monthly average ozone during April is shown in Fig. 3a
210 (upper panel) for the three different emission inventories (HTAP, INTEX, and SEAC4RS). Generally the months
211 of March and May are marked with seasonal transition from winter to summer and summer to monsoon
212 respectively. Hence, the month of April is chosen to represent the pre-monsoon season as it is not influenced by
213 these seasonal transitions, and the observational data is available for a maximum number of stations during this
214 month for the comparison. The 24-h average ozone mixing ratios are found to be 40-55 ppbv over most of the
215 Indian subcontinent for all the three inventories. Model simulated ozone levels over the coastal regions are also
216 similar (30-40 ppbv) among the three inventories. The highest ozone mixing ratios (55 ppbv and higher) predicted
217 in the South Asian region are found over northern India and the Tibetan Plateau. The WRF-Chem simulated
218 spatial distributions of average ozone shown here are in agreement with a previous evaluation study over South
219 Asia (Kumar et al., 2012b). Further, it is found that qualitatively as well as quantitatively the HTAP, INTEX-B
220 and SEAC4RS lead to very similar distributions of 24-h average ozone over most of the South Asian region. The
221 24h monthly average ozone from observations is superimposed on the model results in Fig. 3a for comparison.
222 WRF-Chem simulated distributions of average O₃ are in general agreement with the observational data (Fig. 3a),
223 except at a few stations near coasts (e. g. Kannur and Thumba) and in complex terrain (Pantnagar and Dibrugarh).
224 In contrast to the distribution of 24-h average O₃, the noontime (1130-1630 IST) O₃ mixing ratios over continental
225 South Asia exhibit significant differences among the three emission inventories (Fig. 3b). HTAP clearly leads to
226 higher noontime O₃ mixing ratios, the difference being up to 10 ppbv over the Indo-Gangetic plain (IGP), 20 ppbv
227 over Central India, 30 ppbv over Southern India, compared to INTEX-B and SEAC4RS. The mean bias (MB)
228 (model-observation) for 24-h and noontime average ozone at individual stations is provided in the supplementary
229 material - Table S1 and S2.

230

231 The net photochemical O₃ production rate (ppbv h⁻¹) from sunrise to noontime (0630-1230 IST), when most of the
232 photochemical build-up of ozone takes place and leading to its peak noontime mixing ratio, has been calculated
233 utilizing the chemical tendencies in WRF-Chem (Barth et al., 2012; Girach et al., 2016). A comparison of monthly
234 average O₃ production rates among the three inventories is shown in Fig. 4. As seen also from the O₃ mixing ratios



235 (Fig. 3b), the HTAP emissions result in faster O_3 production ($\sim 9 \text{ ppbv h}^{-1}$) throughout the IGP region. The highest
236 O_3 production rates for INTEX-B and SEAC4RS inventories are simulated only in the East Indian regions
237 including the eastern parts of the IGP. It is noted that the rate of O_3 production is lower ($4\text{--}8 \text{ ppbv h}^{-1}$) over most of
238 the south-western IGP for the INTEX-B and SEAC4RS inventories. Differences are also found over the southern
239 Indian region with stronger ozone production in HTAP, followed by INTEX-B and SEAC4RS.

240

241 Figure 5 provides insight into the spatial distribution of O_3 production regimes estimated through the CH_2O/NO_y
242 ratio (Geng et al., 2007; Kumar et al. 2012b) calculated during 0630 – 1230 IST, to help explain the differences in
243 modelled ozone mixing ratios among the three simulations. The spatial distribution of regimes in all simulations is
244 largely consistent with the findings of Kumar et al. (2012b) although the latter performed the analysis for
245 afternoon hours (1130 – 1430 IST). The S4RS-RADM2 simulation predicts the entire IGP to be VOC sensitive
246 whereas in HTAP-RADM2 and INTEX-RADM2 simulations though the northwest IGP and eastern IGP are VOC
247 sensitive, the central IGP is mostly NO_x limited. The coastal regions are also predicted to be VOC limited in all the
248 three simulations. With the north-western IGP being VOC limited in all simulations, the noontime ozone mixing
249 ratios are found to be higher in this region in HTAP-RADM2 simulation because of high NMVOC emissions in
250 HTAP inventory as evident from figure 2 and table 2. Similar differences are also apparent in southern India.

251

252 In summary, these results show similar 24-h average ozone distributions but large differences in the ozone build-
253 up until noon. The net photochemical ozone production in the morning hours (0630–1230) is shown to be sensitive
254 to the different inventories over this region, which is attributed to differences in total NO_x and/or NMVOC
255 emissions. We therefore suggest that a focus on 24-h averages only would be insufficient to evaluate the ozone
256 budget and implications for human health and crops. Next we compare the modeled diurnal ozone variations from
257 three inventories with in situ measurements over 18 stations across the South Asia.

258

259 3.2. Diurnal variation

260 A comparison of WRF-Chem simulated diurnal ozone variability with recent in situ measurements over a network
261 of 18 stations in the South Asian region is shown in Fig. 6. WRF-Chem is found to successfully reproduce the
262 characteristic diurnal ozone patterns observed over the urban (e.g. Mohali, Delhi, Kanpur, Ahmedabad,
263 Bhubaneswar and Pune) and rural (e.g. Joharapur, Anantpur, Gadanki) stations, indicating strong ozone build-up
264 from sunrise to noontime and the predominance of chemical titration (by NO) and deposition losses during the
265 night. In general, WRF-Chem captures the daily amplitude of O_3 changes at relatively cleaner and high altitude
266 stations, typically showing less pronounced diurnal variability, such as Nainital in the Himalayas and Mt. Abu in
267 the Aravalli mountain range, although with differences in timing when model and observations attain minimum
268 ozone mixing ratios, thus leading to relatively low correlation coefficient (see later in the text). For example,
269 modelled diurnal amplitudes at Nainital are estimated to be $\sim 19.2 \text{ ppbv}$ (HTAP-RADM2), $\sim 17.5 \text{ ppbv}$ (INTEX-
270 RADM2) and $\sim 17.9 \text{ ppbv}$ (S4RS-RADM2) as compared to the observational value of $\sim 15.1 \text{ ppbv}$. The model does
271 not reproduce the ozone mixing ratios at Pantnagar and Jabalpur except for afternoon peak values. This can be
272 attributed to the role of complex terrain (presence of the Himalayas near Pantnagar), which cannot be fully
273 resolved, even at 12 km resolution. Jabalpur is also surrounded by forests, hills and mountains (Sarkar et al.,
274 2015), and such variability in a small area could impact the accuracy of model predictions. The model typically



275 overestimates the noontime ozone mixing ratios over several urban (e.g. Kanpur, Ahmedabad, Haldia, Thumba)
276 and rural stations (e.g. Johrapur, Kannur), which is attributed to the uncertainties in the emissions.

277 To briefly evaluate the possible effects due to the difference in meteorological year between model and
278 observations, we repeated the HTAP-RADM2 simulation for a different year (2010) as shown in the
279 Supplementary material – Fig. S3. The effect of changing the meteorological year in the model simulation is
280 generally small (mostly within ± 3 ppbv in 3 years), except at a few stations in the east (Haldia and Bhubaneswar)
281 and north (Nainital and Pantnagar). The effect is seen to vary from 4.8 ppbv to 11 ppbv (in 3 years) at these four
282 stations. These differences are found to be associated with the inter-annual variations in the regional and
283 transported biomass burning emissions, as seen from MODIS fire counts and MOZART/GEOS5 boundary
284 conditions (not shown).

285 The model ability to reproduce diurnal variations at all stations is summarised using a Taylor diagram (Taylor,
286 2001) in Figure 7. The statistics presented are normalised standard deviation (SD), normalised centred root mean
287 squared difference (RMSD) and the correlation coefficient. The normalisation of both SD and RMSD is done
288 using the standard deviation of the respective observational data. The point indicated as ‘REF’ represents the
289 observational data against the model results evaluated. WRF-Chem simulations show reasonable agreement with
290 observations with correlation coefficients generally greater than 0.7 for most sites. The locations such as Nainital,
291 Mt. Abu and Jabalpur for which r values are lower (0.3-0.7) are associated with unresolved complex terrain, as
292 mentioned earlier.

293 4. Effects of chemical mechanism (RADM2 vs MOZART)

294 A recent WRF-Chem evaluation over Europe showed better agreement with in situ measurements when the
295 MOZART chemical mechanism was employed, compared to RADM2 (Mar et al., 2016). Following up on this,
296 here we compare modelled ozone mixing ratios obtained with these two extensively used chemical mechanisms
297 over South Asia: RADM2 (e. g. Kumar et al., 2012b; Michael et al., 2013; Ojha et al., 2016, Girach et al., 2016)
298 and MOZART (e. g. Ghude et al., 2014; Ghude et al., 2016), keeping the same input emission inventory (HTAP).
299 Thus, the following sensitivity analysis is aimed at exploring if the use of the more detailed chemical mechanism
300 of MOZART could improve the model performance.

301 4.1. Spatial distribution of surface O_3

302 The WRF-Chem simulated spatial distributions of 24-h average and noontime average surface ozone are compared
303 in Fig. 8. The monthly values of the 24-h and noontime ozone mixing ratios from measurements are also shown.
304 Overall, the average ozone mixing ratios over South Asia are simulated to be higher with the MOZART chemical
305 mechanism compared to RADM2, which is consistent with the results of Mar et al. (2016) for the European
306 domain. The 24-h average ozone mixing ratios over India simulated with MOZART chemistry are found to be
307 higher than those with RADM2 chemistry, especially over the eastern Indian region (~ 60 ppbv and more for
308 MOZART compared to ~ 40 -55 ppbv for RADM2). Average ozone levels over the coastal regions are found to be
309 similar between the two mechanisms (30-40 ppbv). MOZART chemistry also predicts high 24-h average ozone
310 mixing ratios (55 ppbv and higher) over the Tibetan Plateau region, similar to RADM2. A striking difference
311 between the two chemical mechanisms is found over the marine regions adjacent to South Asia (Bay of Bengal
312 and northern Indian Ocean), with MOZART predicting significantly higher 24-h average ozone levels (35-50
313 ppbv) compared to the RADM2 (25-40 ppbv). A comparison of noontime average ozone distributions between the



314 two chemical mechanism shows that MOZART predicts higher ozone concentrations than RADM2 over most of
315 the Indian region by about 5-20 ppbv, except over western India. The differences are up to 20 ppbv and more over
316 the Southern Indian region, highlighting the impacts of chemical mechanisms on modelled ozone in this region.
317 The mean bias (MB) values (model-observation) for 24-h and noontime average ozone at individual stations is
318 provided in the supplementary material - Table S1 and S2.

319

320 Figure 9a shows a comparison of the monthly average chemical O₃ tendency (ppbv h⁻¹) from 0630 to 1230 IST. In
321 contrast with average O₃ mixing ratios, which were found to be higher in HTAP-MOZ, the net O₃ production rates
322 at the surface are higher in HTAP-RADM2 over most of the domain, especially in the IGP and central India. The
323 net O₃ production rates at the surface with HTAP-RADM2 are found to be 6 to 9 ppbv h⁻¹ and more over the IGP,
324 whereas these values are generally lower in HTAP-MOZ (4-8 ppbv h⁻¹), except in the north-eastern IGP (>9 ppbv
325 h⁻¹). Fig. 9b shows the sum of the chemical tendency and vertical mixing tendency at the surface for the HTAP-
326 RADM2 and HTAP-MOZ. Analysis of the vertical mixing tendency revealed that higher surface ozone mixing
327 ratios in the MOZART simulation are due to mixing with ozone rich air from aloft. In the HTAP-RADM2
328 simulation, vertical mixing dilutes the effect of strong chemical surface ozone production. Further analysis of
329 vertical distributions of chemical O₃ tendencies reveals stronger photochemical production of ozone aloft with
330 MOZART compared to RADM2 (Supplementary material-Fig. S4). This leads to higher ozone mixing ratios aloft
331 in MOZART simulations.

332 Mar et al. (2016) showed that RADM2 exhibits greater VOC sensitivity than MOZART (i.e., producing higher
333 changes in ozone given a perturbation in VOC emissions) under noontime summer conditions over Europe. This is
334 consistent with our findings as well, that the net surface photochemical ozone production is greater for HTAP-
335 RADM2 than for HTAP-MOZART, given the high VOC emissions in the HTAP inventory. At the surface, the
336 MOZART mechanism predicts larger areas of VOC-sensitivity (as diagnosed by the CH₂O/NO_y indicator, Figure
337 10) and lower net photochemical ozone production than RADM2. With increasing altitude, both the HTAP-
338 RADM2 and HTAP-MOZART simulations show a general increase of CH₂O/NO_y over India, i.e. the chemistry
339 tends to exhibit increased NO_x sensitivity with increasing height (Supplementary material-Figure S6). At model
340 levels above the surface, HTAP-MOZART shows greater net photochemical production of ozone than HTAP-
341 RADM2 (Supplementary material-Figure S4), which is what Mar et al. (2016) have also reported for the surface
342 O₃ over Europe. When these effects are combined, mixing leads to higher surface ozone mixing ratios for HTAP-
343 MOZART than for HTAP-RADM2. The differences in ozone mixing ratios between the MOZART and RADM2
344 chemical mechanisms can be attributed to the additional chemical species and reactions, differences in the rate
345 constants for several inorganic reactions, and photolysis schemes used, with relatively smaller effects from O₃ dry
346 deposition (as in Mar et al. 2016). Our analysis also shows the importance of chemical regime in understanding
347 differences between the chemical mechanisms, and highlights the significant effects of the employed chemical
348 mechanism on modelled ozone over South Asia.

349 4.2. Diurnal variation

350 Figure 11 shows a comparison of WRF-Chem simulated ozone variations on diurnal timescales with recent in situ
351 measurements over a network of stations across the South Asia for the two chemical mechanisms (MOZART and
352 RADM2); again with the same emission inventory (HTAP). Qualitatively, both simulations produce very similar
353 diurnal patterns, however, the absolute O₃ mixing ratios are found to differ significantly between the two chemical



354 mechanisms. Noontime ozone mixing ratios predicted by MOZART are either significantly higher (at 12 out of 18
355 stations) or nearly similar (at 6 stations). MOZART-predicted O₃ at Dibrugarh, Kanpur, Jabalpur, Bhubaneswar,
356 Gadanki and Thumba was found to be higher by ~12 ppbv, 5 ppbv, 8 ppbv, 10 ppbv, 11 ppbv and 12 ppbv,
357 respectively, compared to RADM2 (Supplementary material, Table S2). Over several urban and rural stations in
358 India (e.g. Delhi, Ahmedabad, Pune, Kannur and Thumba) MOZART is found to titrate ozone more strongly
359 during the night while resulting in higher or similar ozone levels around noon. The contrasting comparison
360 between noon and night time found at these sites suggests that evaluation limited to 24 h averages would not be
361 sufficient, and that model performance on a diurnal time scale should be considered to assess the photochemical
362 build-up of O₃.

363

364 In general, the noontime ozone mixing ratios predicted by RADM2 are found to be in better agreement with in situ
365 measurements compared to MOZART. The model performance of two chemical mechanisms in reproducing
366 diurnal variation at all stations is summarised using a Taylor diagram in Fig. 12. Both chemical mechanisms show
367 reasonably good agreement ($r > 0.7$) at most of the sites, except two stations associated with highly complex
368 terrain (Nainital and Mt. Abu). On the Taylor diagram, most of the HTAP-RADM2 results are found to be closer
369 to the 'REF', as compared to HTAP-MOZ results, suggesting that the RADM2 chemical mechanism is better
370 suited to simulate ozone over this region.

371

372 5. Overall evaluation and recommendations

373 In this section, we present a sub-regional evaluation of all simulations by subdividing the domain into five
374 geographical areas, i.e. North, South, East, West and central India, as shown in Fig. 1. The recommendations for
375 the individual stations based on the model evaluation are summarized in the Supplementary material (Table S1 and
376 S2). The temporal correlation coefficients of diurnally varying O₃, spatially averaged over each of the five
377 different sub-regions, are found to be reasonably high, generally exceeding 0.7 (Table 5). The r values for
378 individual sub-regions are found to be similar among the four simulations. For example, over north India the r
379 values vary from 0.86 to 0.90. The model performance differs among several sub-regions, with correlations being
380 lower for central India ($r = 0.67-0.75$). Since the latter is based on only one station associated with complex terrain
381 (Jabalpur), we suggest that observations over additional stations should be conducted to evaluate the model
382 performance in the central Indian region. As correlations are similar among different simulations, we focus on the
383 mean bias values especially around noontime (Table 6). Amongst the four different combinations of simulations
384 performed we find HTAP-RADM2 yields lowest noontime biases over north (MB = ~2.4 ppbv) and central India
385 (~0.9 ppbv). The S4RS-RADM2 combination is recommended for the east (MB ~15.3 ppbv) and South (MB ~6.5
386 ppbv) Indian regions. On the other hand, INTEX-RADM2 is found to yield better agreement with measurements
387 over western India (MB = ~8 ppbv). The recommendation for each region based solely on the ability to predict
388 noontime O₃ concentrations is summarized in table 7. These results show that the performance of emission
389 inventories is regionally different, and that these biases should be considered in utilizing model for assessment of
390 air quality and impacts on human health and crop yields.

391

392 We finally evaluate the different simulations in the context of the entire south Asian region. Figure 13 shows a
393 comparison of model results and measurements with diurnal box/whisker plots, combining all stations for the four
394 different simulations. As mentioned earlier, noontime ozone levels are overestimated by all four simulations. The



395 overestimation of noontime ozone is found to be largest in the HTAP-MOZ simulation, followed by HTAP-
396 RADM2, and lowest with S4RS-RADM2. These results further suggest that assessment of the tropospheric ozone
397 budget as well as implications for public health and crop loss are associated with considerable uncertainty, and
398 biases need to be considered. A recent study (Ghude et al., 2016), for example, subtracted 15 ppbv from the WRF-
399 Chem simulated ozone mixing ratios before deriving premature mortalities over the Indian region. The results of
400 this study are summarized in the form of a polar plot (Fig. 14) showing the monthly mean diurnal variation from
401 all runs for the entire south Asian domain. The noontime normalized mean bias values with respect to observed
402 values are ~11% (S4RS-RADM2), ~12.5% (INTEX-RADM2), ~22% (HTAP-RADM2) and ~36.5% (HTAP-
403 MOZ). It is interesting to note that the SEAC4RS inventory (representative of year 2012) yields quite similar
404 results as the INTEX-B inventory (representative of year 2006). It is concluded that the SEAC4RS inventory,
405 which is the most recent inventory amongst the three inventories considered in this study, is best suited for O₃
406 prediction over south Asian region as a whole in combination with RADM2 Chemistry.

407

408 **6. Summary and conclusions**

409 In this paper, we evaluated the WRF-Chem simulated surface ozone over South Asia during the pre-monsoon
410 season against recent in situ measurements from a network of 18 stations, employing three different inventories
411 (EDGAR-HTAP, INTEX-B, and SEAC4RS) for anthropogenic emissions with the RADM2 chemical mechanism.
412 WRF-Chem simulated ozone distributions showed highest ozone mixing ratios (~55 ppbv and higher) over
413 northern India and the Tibetan Plateau. In general, modelled average ozone distributions from different inventories
414 are found to be in agreement with previous studies over this region. Evaluation on diurnal time scales
415 demonstrates the ability of the model to reproduce observed O₃ patterns at urban and rural stations, showing strong
416 noontime ozone build-up and chemical titration and deposition loss during the night-time. WRF-Chem also
417 captures the smaller diurnal amplitudes observed over high altitude, relatively pristine stations. However, model
418 showed limitations in capturing ozone mixing ratios in the vicinity of the complex terrain, indicating that even a
419 relatively high horizontal resolution of 12 km x 12 km could not fully resolve the topography induced effects.

420 Overall WRF-Chem simulations show reasonable agreement with observations, with correlation coefficients
421 generally higher than 0.7 for most of the sites. It is found that the HTAP, INTEX-B and SEAC4RS inventories
422 lead to very similar distributions of 24-h average ozone over this region. However, noontime (1130-1630 IST) O₃
423 mixing ratios over continental South Asia differ significantly among the three inventories. HTAP inventory
424 generally leads to noontime O₃ mixing ratios higher by 10 ppbv over the Indo-Gangetic plain (IGP), 20 ppbv over
425 Central India, and 30 ppbv over Southern India, compared to the INTEX-B and SEAC4RS inventories. A
426 comparison of monthly average O₃ net production rate during 0630-1230 IST among the three inventories shows
427 that the HTAP emissions result in faster O₃ production (~9 ppbv h⁻¹) throughout the IGP region compared to the
428 other two inventories. Differences are also found over the southern Indian region with stronger ozone production
429 in HTAP, followed by INTEX-B and SEAC4RS. The results show similar 24-h average ozone distributions, but
430 large differences in noontime ozone build up, pointing to the uncertainties in emission inventories over this region.

431 We further investigated the sensitivity of modelled ozone to two extensively used chemical mechanisms, RADM2
432 and MOZART, and maintaining the HTAP emissions. Noontime average surface ozone distributions predicted by
433 MOZART show significant enhancements (10-15 ppbv) with respect to RADM2 over most of the Indian region,
434 except over western India. MOZART predicts higher ozone concentrations than RADM2 by up to 20 ppbv and



435 more over the South Indian region. Monthly average ozone mixing ratios are predicted to be higher by the
436 MOZART chemical mechanism compared to RADM2, as was also found over Europe (Mar et al., 2016). The
437 differences in ozone production between the MOZART and RADM2 chemical mechanisms are mainly attributed
438 to the additional chemical species and reactions, differences in the rate constants for several inorganic reactions,
439 and photolysis schemes used. A comparison of the monthly average chemical O₃ tendency (ppbv h⁻¹) during 0630-
440 1230 IST shows that in contrast with average O₃ mixing ratios, which were found to be higher in MOZART, the
441 net O₃ production rates at the surface are higher with RADM2 chemistry, especially over the IGP and central
442 India. The net O₃ production rates at the surface with RADM2 are found to be 6 to 9 ppbv h⁻¹, and higher over the
443 IGP, whereas these rates are generally lower with MOZART (4-8 ppbv h⁻¹), except in the northeastern IGP (>9
444 ppbv h⁻¹). Analysis of the vertical mixing tendency revealed that higher surface ozone mixing ratios in the
445 MOZART simulation are due to mixing with ozone rich air from aloft. Analysis of vertical distributions of
446 chemical O₃ tendencies reveals stronger photochemical production of ozone aloft with MOZART compared to
447 RADM2. Our analysis highlights the significant effects of the employed chemical mechanism on model predicted
448 ozone over South Asia.

449 Qualitatively, RADM2 and MOZART simulations predict similar diurnal patterns; however the absolute O₃
450 mixing ratios differ significantly. Noontime ozone mixing ratios predicted by MOZART are significantly higher at
451 12 out of 18 stations, while these were found to be similar at 6 stations. Over several urban and rural stations in
452 India MOZART is found to titrate ozone relatively strongly during the night, while producing higher or similar
453 ozone levels during noontime compared to RADM2. The contrasting evaluation results between day- (noon) and
454 night-time could counterbalance in evaluation studies limited to 24 h averages, possibly showing better agreement
455 and therefore hence it is pertinent to consider the diurnally resolved model performance. In general, the noontime
456 ozone mixing ratios predicted by RADM2 are found to be in better agreement with in situ measurements at the
457 surface compared to MOZART.

458 Model evaluation over different geographical regions in South Asia reveals strong spatial heterogeneity in the
459 WRF-Chem performance. SEAC4RS inventory leads to better agreement with observations over east (MB = ~15.3
460 ppbv) and south India (~6.5 ppbv), whereas the HTAP inventory performs better over north (MB = ~2.4 ppbv) and
461 central India (~0.9 ppbv), and INTEX-B over west India (MB = ~8 ppbv). For the entire region, the overestimation
462 of noontime ozone is found to be highest with the HTAP inventory (with the MOZART chemical mechanism) and
463 lowest with the SEAC4RS inventory. The noontime normalized mean bias is lowest for the SEAC4RS inventory
464 with the RADM2 chemical mechanism (~11%), followed by INTEX-B with RADM2 (~12.5%), HTAP with
465 RADM2 (~22%), and HTAP with MOZART (~36.5%). These results further suggest that the assessment of the
466 tropospheric ozone budget and consequently its implications on public health and agricultural output should be
467 carried out cautiously by considering the large uncertainties associated with use of emission inventories and
468 chemical mechanism incorporated. It is interesting to note that the SEAC4RS inventory (representative of 2012)
469 yields results comparable to the INTEX-B inventory (for 2006), even though the SECA4RS inventory has about
470 46% higher NO_x, 9% higher NMVOC and 15% lower CO emissions compared to INTEX-B. We conclude that the
471 SEAC4RS inventory, the most recent inventory amongst the three inventories, is best suited for O₃ prediction over
472 south Asian region as a whole in combination with RADM2 Chemistry. Our study highlights the need to also
473 evaluate O₃ precursors, similar to that conducted here for ozone, to further reduce uncertainties in modelled ozone
474 over South Asia for the better assessment of implications of surface ozone on public health and crop yield.



475 **Data availability:** The model output from all the numerical simulations is available at the MPG supercomputer
476 HYDRA (<http://www.mpcdf.mpg.de/services/computing/hydra>) and would be provided by contacting the
477 corresponding authors. The observed values shown for comparison are from previous papers with complete list of
478 references provided in the Table 4. New observations for Delhi and Pune stations are available from the SAFAR
479 program (<http://safar.tropmet.res.in/>).

480 **Acknowledgement**

481 A. Sharma acknowledges the fellowship from the Max Planck Institute for Chemistry to carry out this study. S. S.
482 Gunthe acknowledges the support from DST-Max Planck partner group at IIT Madras and Ministry of Earth
483 Sciences (MoES), Govt. of India. Model simulations have been performed on the MPG supercomputer HYDRA
484 (<http://www.mpcdf.mpg.de/services/computing/hydra>). Initial and boundary conditions data for meteorological
485 fields were obtained from ECMWF website (<http://www.ecmwf.int/en/research/climate-reanalysis/era-interim>).
486 The HTAP v2 anthropogenic emissions were obtained from [http://edgar.jrc.ec.europa.eu/htap_v2/](http://edgar.jrc.ec.europa.eu/htap_v2/index.php?SECURE=123)
487 [index.php?SECURE=123](http://edgar.jrc.ec.europa.eu/htap_v2/index.php?SECURE=123). Authors are grateful to Yafang Cheng (MPI-C) for providing SEAC4RS emission. The
488 INTEX-B anthropogenic emissions were obtained from [http://bio.cgrer.uiowa.edu/EMISSION_DATA_new](http://bio.cgrer.uiowa.edu/EMISSION_DATA_new/data/intex-b_emissions/)
489 [/data/intex-b_emissions/](http://bio.cgrer.uiowa.edu/EMISSION_DATA_new/data/intex-b_emissions/). MOZART-4/ GEOS5 output used as initial and boundary conditions for chemical fields
490 is acknowledged. The pre-processors and inputs for biogenic and biomass-burning emissions were obtained from
491 NCAR Atmospheric Chemistry website (<http://www.acd.ucar.edu/wrf-chem/>). Authors are also thankful for the
492 usage of HPC supercluster and to the staff at P. G. Senapathy Computer Center at IIT Madras.

493 **References**

- 494 Ackermann, I. J., Hass, H., Memmesheimer, M., Ebel, A., Binkowski, F. S., and Shankar, U.: Modal aerosol
495 dynamics model for Europe: development and first applications, *Atmos. Environ.*, 32, 2981–2999,
496 doi:10.1016/S1352-2310(98)00006-5, 1998.
- 497 Ainsworth, E. A., Yendrek, C. R., Sitch, S., Collins, W. J., and Emberson, L. D.: The effects of tropospheric ozone
498 on net primary productivity and implications for climate change, *Ann. Rev. Plant Biol.*, 63, 637–661, 2012.
- 499 Akimoto, H.: Global air quality and pollution, *Science*, 302, 1716–1719, doi:10.1126/science.1092666, 2003.
- 500 Amnuaylojaroen, T., Barth, M. C., Emmons, L. K., Carmichael, G. R., Kreasuwun, J., Prasitwattanaseree, S., and
501 Chantara, S.: Effect of different emission inventories on modeled ozone and carbon monoxide in Southeast Asia,
502 *Atmos. Chem. Phys.*, 14, 12983–13012, doi:10.5194/acp-14-12983-2014, 2014.
- 503 Anenberg, S. C., Horowitz, L. W., Tong, D. Q., and West, J. J.: An estimate of the global burden of anthropogenic
504 ozone and fine particulate matter on premature human mortality using atmospheric modelling, *Environmental*
505 *Health Perspectives*, 118, 1189–1195, 2010.
- 506 Ansari, T. U., Ojha, N., Chandrasekar, R., Balaji, C., Singh, N. and Gunthe, S. S.: Competing impact of
507 anthropogenic emissions and meteorology on the distribution of trace gases over Indian region, *J. Atmos. Chem.*,
508 doi:10.1007/s10874-016-9331-y, 2016.
- 509 Atkinson, R.: Atmospheric chemistry of VOCs and NO_x, *Atmos. Environ.*, 34, 2063–2101, doi:10.1016/S1352-
510 2310(99)00460-4, 2000.



- 511 Barth, M. C., Lee, J., Hodzic, A., Pfister, G., Skamarock, W. C., Worden, J., Wong, J., and Noone, D.:
512 Thunderstorms and upper troposphere chemistry during the early stages of the 2006 North American Monsoon,
513 Atmos. Chem. Phys., 12, 11003-11026, doi:10.5194/acp-12-11003-2012, 2012.
- 514 Bell, M. L., McDermott, A., Zeger, S. L., Samet, J. M., and Dominici, F.: Ozone and short term mortality in 95 US
515 urban communities, 1987-2000, JAMA The Journal of the American Medical Association, 292, 2372-2378, 2004.
- 516 Bhuyan, P.K., Bharali, C., Pathak, B., and Kalita, G.: The role of precursor gases and meteorology on temporal
517 evolution of O₃ at a tropical location in northeast India, Environmental Science and Pollution Research, 21, 6696–
518 6713, 2014.
- 519 Carmichael, G. R., Sakurai, T., Streets, D., Hozumi, Y., Ueda, H., Park, S. U., Funge, C., Han, Z., Kajino, M.,
520 Engardt, M., Bennet, C., Hayami, H., Sartelet, K., Holloway, T., Wang, Z., Kannari, A., Fu, J., Matsuda, K.,
521 Thongboonchoo, N., and Amann, M.: MICS-Asia II: the model intercomparison study for Asia Phase II
522 methodology and overview of findings, Atmos. Environ., 42, 3468–3490, doi:10.1016/j.atmosenv.2007.04.007,
523 2008.
- 524 Chin, M., Rood, R. B., Lin, S. -J., Muller, J. F., and Thomson, A. M.: Atmospheric sulfur cycle in the global
525 model GOCART: Model description and global properties, J. Geophys. Res., 105, 24,671-24,687, 2000.
- 526 Chou, M. -D., and Suarez, M. J.: An efficient thermal infrared radiation parameterization for use in general
527 circulation models, NASA Technical Memorandum 104606, 3, 85pp, 1994.
- 528 Cox, R. A., Eggleton, A. E. J., Derwent, R. G., Lovelock, J. E., and Pack, D. H.: Long-range transport of
529 photochemical ozone in north-western Europe, Nature, 255, 118 – 121, doi:10.1038/255118a0, 1975.
- 530 Crutzen, P. J.: Photochemical reactions initiated by and influencing ozone in unpolluted tropospheric air, Tellus,
531 26, 47–57, 1974.
- 532 David, L. M., and Nair, P. R.: Diurnal and seasonal variability of surface ozone and NO_x at a tropical coastal site:
533 association with mesoscale and synoptic meteorological conditions, Journal of Geophysical Research 116,
534 D10303. <http://dx.doi.org/10.1029/2010JD015076>, 2011.
- 535 Debaje, S. B., and Kakade, A. D.: Measurements of Surface Ozone in Rural Site of India, Aerosol and Air Quality
536 Research, Vol. 6, No. 4, pp. 444-465, 2006.
- 537 Dumka, U. C., Krishna Moorthy, K., Kumar, R., Hegde, P., Sagar, R., Pant, P., Singh, N., and Suresh Babu, S.:
538 Characteristics of aerosol black carbon mass concentration over a high altitude location in the central Himalayas
539 from multi-year measurements, Atmos. Res., 96, 510–521, 2010.
- 540 Emberson, L. D., Buker, P., Ashmore, M., Mills, G., Jackson, L., Agrawal, M., Atikuzzaman, M., Cinderby, S.,
541 Engardt, M., Jamir, C., Kobayashi, K., Oanh, N., Quadir, Q., and Wahid, A.: A comparison of North-American
542 and Asian exposure-response data for ozone effects on crop yields, Atmos. Environ., 43, 1945–1953, 2009.
- 543 Emmons, L. K., Walters, S., Hess, P. G., Lamarque, J.-F., Pfister, G. G., Fillmore, D., Granier, C., Guenther, A.,
544 Kinnison, D., Laepple, T., Orlando, J., Tie, X., Tyndall, G., Wiedinmyer, C., Baughcum, S. L., and Kloster, S.:



- 545 Description and evaluation of the Model for Ozone and Related chemical Tracers, version 4 (MOZART-4),
546 Geosci. Model Dev., 3, 43–67, 20 doi:10.5194/gmd-3-43-2010, 2010.
- 547 Fast, J. D., Gustafson Jr., W. I., Easter, R. C., Zaveri, R. A., Barnard, J. C., Chapman, E. G., Grell, G. A. and
548 Peckham, S. E.: Evolution of ozone, particulates, and aerosol direct radiative forcing in the vicinity of Houston
549 using a fully-coupled meteorology-chemistry aerosol model, Journal of Geophysical Research, 111, D21305,
550 2006.
- 551 Gaur, A., Tripathi, S. N., Kanawade, V. P., Tare, V., and Shukla, S. P.: Four-year measurements of trace gases
552 (SO₂, NO_x, CO, and O₃) at an urban location, Kanpur, in Northern India, J. Atmos. Chem., 71, 283–301, 2014.
- 553 Geng, F., Zhao, C., Tang, X., Lu, G., and Tie, X.: Analysis of ozone and VOCs measured in Shanghai: A case
554 study, Atmos. Environ., 41, 989–1001, 2007.
- 555 Ghude, S. D., Jena, C., Chate, D. M., Beig, G., Pfister, G. G., Kumar, R., and Ramanathan, V.: Reduction in
556 India's crop yield due to ozone, Geophys. Res. Lett., 41, 51971, doi:10.1002/2014GL060930, 2014.
- 557 Ghude, S. D., Chate, D. M., Jena, C., Beig, G., Kumar, R., Barth, M. C., Pfister, G. G., Fadnavis, S. and Pithani,
558 P.: Premature mortality in India due to PM_{2.5} and ozone exposure, Geophysical Research Letters, 4650 – 4658,
559 2016.
- 560 Girach, I. A., Ojha, N., Nair, P. R., Pozzer, A., Tiwari, Y. K., Kumar, K. R., and Lelieveld, J.: Variations in O₃,
561 CO, and CH₄ over the Bay of Bengal during the summer monsoon season: Ship-borne measurements and model
562 simulations, Atmos. Chem. Phys. Discuss., doi:10.5194/acp-2016-595, in review, 2016.
- 563 Grell, G.: Prognostic evaluation of assumptions used by cumulus parameterizations, Monthly Weather Review,
564 121, 764-787, 1993.
- 565 Grell, G., and Devenyi, D.: A generalized approach to parameterizing convection combining ensemble and data
566 assimilation techniques, Geophys. Res. Lett., 29(14), 38–31, 2002.
- 567 Grell, G. A., Peckham, S. E., McKeen, S., Schmitz, R., Frost, G., Skamarock, W. C. and Eder, B.: Fully coupled
568 'online' chemistry within the WRF model, Atmospheric Environment, 39, 6957–6975, 2005.
- 569 Gupta, M. and Mohan, M.: Validation of WRF/Chem model and sensitivity of chemical mechanisms to ozone
570 simulation over megacity Delhi, Atmospheric Environment, Volume 122, p. 220-229, 2015.
- 571 Guenther, A., Karl, T., Harley, P., Wiedinmyer, C., Palmer, P. I., and Geron, C.: Estimates of global terrestrial
572 isoprene emissions using MEGAN (Model of Emissions of Gases and Aerosols from Nature), Atmos. Chem.
573 Phys., 6, 3181–3210, doi:10.5194/acp-6-3181-2006, 2006.
- 574 Gurjar, B. R., Ravindra, K., and Nagpure, A.S.: Air pollution trends over Indian megacities and their local-to-
575 global implications, Atmospheric Environment, Volume 142, Pages 475–495,
576 <http://dx.doi.org/10.1016/j.atmosenv.2016.06.030>, 2016.



- 577 Jain, S. L., Arya, B. C., Kumar, A., Ghude, S. D., and Kulkarni, P. S.: Observational study of surface ozone at
578 New Delhi, India, *Int. J. Remote Sens.*, 26, 3515–3524, 2005.
- 579 Janjic, Z. I.: The step-mountain eta coordinate model: further developments of the convection, viscous sublayer
580 and turbulence closure schemes, *Monthly Weather Review* 122, 927–945, 1994.
- 581 Janjic, Z. I.: The surface layer in the NCEP Eta Model, Eleventh Conference on Numerical Weather Prediction,
582 Norfolk, VA, 19–23 August; American Meteorological Society, Boston, MA, 354–355, 1996.
- 583 Janjic, Z. I.: Nonsingular Implementation of the Mellor–Yamada Level 2.5 Scheme in the NCEP Meso model,
584 NCEP Office Note, No. 437, 61 pp, 2002.
- 585 Janssens-Maenhout, G., Crippa, M., Guizzardi, D., Dentener, F., Muntean, M., Pouliot, G., Keating, T., Zhang, Q.,
586 Kurokawa, J., Wankmüller, R., Denier van der Gon, H., Kuenen, J. J. P., Klimont, Z., Frost, G., Darras, S., Koffi,
587 B., and Li, M.: HTAP_v2.2: a mosaic of regional and global emission grid maps for 2008 and 2010 to study
588 hemispheric transport of air pollution, *Atmos. Chem. Phys.*, 15, 11411e11432, [http://dx.doi.org/10.5194/acp-15-](http://dx.doi.org/10.5194/acp-15-11411-2015)
589 11411-2015, 2015.
- 590 Jena, C., Ghude, S. D., Beig, G., Chate, D. M., Kumar, R., Pfister, G. G., Lal, D. M., Surendran, D. E., Fadnavis,
591 S., and van der, A. R. J.: Inter-comparison of different NO_x emission inventories and associated variation in
592 simulated surface ozone in Indian region, *Atmos. Environ.*, 117:61–73, 2015.
- 593 Jerrett, M., Burnett, R. T., Pope, C. A., III, Ito, K., Thurston, G., Krewski, D., et al.: Long-term ozone exposure
594 and mortality, *The New England Journal of Medicine*, 360, 1085–1095, 2009.
- 595 Kleinman, L., Lee, Y. -N., Springston, S. R., Nunnermacker, L., Zhou, X., Brown, R., Hallock, K., Klotz, P.,
596 Leahy, D., Lee, J. H., and Newman, L.: Ozone formation at a rural site in the southeastern United States, *J.*
597 *Geophys. Res.-Atmos.*, 99, 3469–3482, doi:10.1029/93JD02991, 1994.
- 598 Krupa, S. V., Nosal, M., and Legge, A. H.: A numerical analysis of the combined open top chamber data from the
599 USA and Europe on ambient ozone and negative crop responses, *Environmental Pollution*, 101, 157–160, 1998.
- 600 Kumar, R., Naja, M., Venkataramani, S., and Wild, O.: Variations in surface ozone at Nainital: A high-altitude site
601 in the central Himalayas, *J. Geophys. Res.*, 115, D16302, doi:10.1029/2009JD013715, 2010.
- 602 Kumar, R., Naja, M., Pfister, G. G., Barth, M. C., and Brasseur, G. P.: Simulations over South Asia using the
603 Weather Research and Forecasting model with Chemistry (WRF-Chem): set-up and meteorological evaluation,
604 *Geoscientific Model Development*, 5, 321-343, 2012a.
- 605 Kumar, R., Naja, M., Pfister, G. G., Barth, M. C., Wiedinmyer, C., and Brasseur, G. P.: Simulations over South
606 Asia using the Weather Research and Forecasting model with Chemistry (WRF-Chem): chemistry evaluation and
607 initial results, *Geoscientific Model Development* 5, 619-648, 2012b.
- 608 Kumar, R., Barth, M. C., Pfister, G. G., Nair, V. S., Ghude, S. D., and Ojha, N.: What controls the seasonal cycle
609 of black carbon aerosols in India?, *J. Geophys. Res. Atmos.*, 120, 7788–7812, doi:10.1002/2015JD023298, 2015.



- 610 Lal, S.: Trace gases over the Indian region, *Indian Journal of Radio and Space Physics*, 36, 556–579, 2007.
- 611 Lawrence, M. G., Rasch, P. J., von Kuhlmann, R., Williams, J., Fischer, H., de Reus, M., Lelieveld, J., Crutzen, P.
612 J., Schultz, M., Stier, P., Huntrieser, H., Heland, J., Stohl, A., Forster, C., Elbern, H., Jakobs, H., and Dickerson,
613 R. R.: Global chemical weather forecasts for field campaign planning: predictions and observations of large-scale
614 features during MINOS, CONTRACE, and INDOEX, *Atmos. Chem. Phys.*, 3, 267–289, doi:10.5194/acp-3-267-
615 2003, 2003.
- 616 Lawrence, M. G. and Lelieveld, J.: Atmospheric pollutant outflow from southern Asia: a review, *Atmos. chem.*
617 *Phys.*, 10, 11017–11096, doi:10.5194/acp-10-11017-2010, 2010.
- 618 Lelieveld, J., and Dentener, F.J.: What controls tropospheric ozone?, *J. Geophys. Res.*, 105, 3531–3551, 2000.
- 619 Lelieveld, J., Berresheim, H., Borrmann, S., Crutzen, P. J., Dentener, F. J., Fischer, H., Feichter, J., Flatau, P. J.,
620 Heland, J., Holzinger, R., Korrmann, R., Lawrence, M. G., Levin, Z., Markowicz, K. M., Mihalopoulos, N.,
621 Minikin, A., Ramanathan, V., de Reus, M., Roelofs, G. J., Scheeren, H. A., Sciare, J., Schlager, H., Schultz, M.,
622 Siegmund, P., Steil, B., Stephanou, E. G., Stier, P., Traub, M., Warneke, C., Williams, J., and Ziereis, H.: Global
623 air pollution crossroads over the Mediterranean, *Science*, 298, 794–799, doi:10.1126/science.1075457, 2002.
- 624 Lelieveld, J., Evans, J. S., Fnais, M., Giannadaki, D., and Pozzer, A.: The contribution of outdoor air pollution
625 sources to premature mortality on a global scale, *Nature*, 525(7569):367–371, 2015.
- 626 Lin, Y.-L., R. D. Farley, R. D. and Orville, H. D.: Bulk parameterization of the snow field in a cloud model, *J.*
627 *Clim. Appl. Meteorol.*, 22, 1065–1092, 1983.
- 628 Liu, Y., Warner, T. T., Bowers, J. F., Carson, L. P., Chen, F., Clough, C. A., Davis, C. A., Egeland, C. H.,
629 Halvorson, S., Huck Jr., T. W., Lachapelle, L., Malone, R. E., Rife, D. L., Sheu, R., -S., Swerdlin, S. P. and
630 Weingarten, D. S.: The operational mesogamma-scale analysis and forecast system of the U.S. Army Test and
631 Evaluation Command. Part 1: Overview of the modeling system, the forecast products, *Journal of applied*
632 *meteorology and climatology* 47, 1077–1092, 2008.
- 633 Logan, J. A., Staehelin, J., Megretskaia, I. A., Cammas, J.-P., Thouret, V., Claude, H., De Backer, H., Steinbacher,
634 M., Scheel, H.-E., Stubi, R., Frohlich, M., and Derwent, R.: Changes in ozone over Europe: Analysis of ozone
635 measurements from sondes, regular aircraft (MOZAIC) and alpine surface sites, *J. Geophys. Res.*, 117, D09301,
636 doi:10.1029/2011JD016952, 2012.
- 637 Lu, Z. and Streets, D. G.: The Southeast Asia Composition, Cloud, Climate Coupling Regional Study Emission
638 Inventory, available at: <http://bio.cgrer.uiowa.edu/SEAC4RS/emission.html>, 2012.
- 639 Lüthi, Z. L., Skerlak, B., Kim, S.-W., Lauer, A., Mues, A., Rupakheti, M., and Kang, S.: Atmospheric brown
640 clouds reach the Tibetan Plateau by crossing the Himalayas, *Atmos. Chem. Phys.*, 15, 6007–6021,
641 doi:10.5194/acp-15-6007-2015, 2015.



- 642 Mahapatra, P. S., Jena, J., Moharana, S., Srichandan, H., Das, T., Roy, C. G., and Das, S. N.: Surface ozone
643 variation at Bhubaneswar and intra-corelationship study with various parameters, *J. Earth Syst. Sci.* 121, 1163–
644 1175, 2012.
- 645 Mallik C., Lal, S., and Venkataramani, S.: Trace gases at a semi-arid urban site in western India: variability and
646 inter-correlations, *J. Atm. Chem.* Vol. 72, p. 143-164, 2015.
- 647 Mar, K. A., Ojha, N., Pozzer, A., and Butler, T. M.: Ozone air quality simulations with WRF-Chem (v3.5.1) over
648 Europe: model evaluation and chemical mechanism comparison, *Geosci. Model Dev.*, 9, 3699-3728,
649 doi:10.5194/gmd-9-3699-2016, 2016.
- 650 Marrapu, P., Cheng, Y., Beig, G., Sahu, S. K., Srinivas, R. and Carmichael, G. R.: Air Quality in Delhi during the
651 Commonwealth Games, *Atmos. Chem. Phys.*, 14:10619–10630, 2014.
- 652 Mellor, G. L., and Yamada, T.: Development of a turbulence closure model for geophysical fluid problems,
653 *Reviews of geophysics and space physics* 20(4), 851–875, 1982.
- 654 Michael, M., Yadav, A., Tripathi, S. N., Kanawade, V. P., Gaur, A., Sadavarte, P. and Venkataraman, C.:
655 Simulation of trace gases and aerosols over the Indian Domain: Evaluation of the WRF-Chem model, *Atmospheric*
656 *Chemistry and Physics Discussion*, 13, 12287-12336, 2013.
- 657 Mlawer, E. J., Taubman, S. J., Brown, P. D., Iacono, M. J. and Clough, S. A.: Radiative transfer for
658 inhomogeneous atmosphere: RRTM, a validated correlated-k model for the long-wave, *Journal of Geophysical*
659 *Research* 102 (D14), 16663–16682, 1997.
- 660 Monin, A. S. and Obukhov, A. M.: Basic laws of turbulent mixing in the surface layer of the atmosphere, *Contrib.*
661 *Geophys. Inst. Acad. Sci., USSR* 24 (151), 163–187, 1954.
- 662 Monks, P. S., Archibald, A. T., Colette, A., Cooper, O., Coyle, M., Derwent, R., Fowler, D., Granier, C., Law, K.
663 S., Mills, G. E., Stevenson, D. S., Tarasova, O., Thouret, V., von Schneidmesser, E., Sommariva, R., Wild, O.,
664 and Williams, M. L.: Tropospheric ozone and its precursors from the urban to the global scale from air quality to
665 short-lived climate forcer, *Atmos. Chem. Phys.*, 15, 8889-8973, doi:10.5194/acp-15-8889-2015, 2015.
- 666 Naja, M., Lal, S., and Chand, D.: Diurnal and seasonal variabilities in surface ozone at a high altitude site Mt Abu
667 (24.6N, 72.7E, 1680 m asl) in India, *Atmospheric Environment* 37, 4205e4215, 2003.
- 668 Nishanth, T., Praseed, K. M., Sathesh Kumar, M. K., and Valsaraj, K. T.: Analysis of Ground Level O₃ and NO_x
669 Measured at Kannur, India. *J Earth Sci Climate Change*, 3:111, doi:10.4172/2157-7617.1000111, 2012.
- 670 Ohara, T., Akimoto, H., Kurokawa, J., Horii, N., Yamaji, K., Yan, X., and Hayasaka, T.: An Asian emission
671 inventory of anthropogenic emission sources for the period 1980–2020, *Atmos. Chem. Phys.*, 7, 4419–4444,
672 doi:10.5194/acp-7-4419-2007, 2007.
- 673 Ojha, N., Naja, M., Singh, K. P., Sarangi, T., Kumar, R., Lal, S., Lawrence, M. G., Butler, T. M., and Chandola,
674 H. C.: Variabilities in ozone at a semi-urban site in the Indo-Gangetic Plain region: Association with the
675 meteorology and regional process, *J. Geophys. Res.*, 117, D20301, doi:10.1029/2012JD017716, 2012.



- 676 Ojha, N., Naja, M., Sarangi, T., Kumar, R., Bhardwaj, P., Lal, S., Venkataramani, S., Sagar, R., Kumar, A., and
677 Chandola, H. C.: On the processes influencing the vertical distribution of ozone over the central Himalayas:
678 Analysis of yearlong ozonesonde observations, *Atmos. Environ.*, 88, 201–211,
679 doi:10.1016/j.atmosenv.2014.01.031, 2014.
- 680 Ojha, N., Pozzer, A., Rauthe-Schöch, A., Baker, A. K., Yoon, J., Brenninkmeijer, C. A. M., and Lelieveld, J.:
681 Ozone and carbon monoxide over India during the summer monsoon: regional emissions and transport, *Atmos.*
682 *Chem. Phys.*, 16, 3013–3032, doi:10.5194/acp-16-3013-2016, 2016.
- 683 Otte, T. L.: The impact of nudging in the meteorological model for retrospective air quality simulations. Part I:
684 Evaluation against national observation networks, *J. Appl. Meteor. Climatol.*, 47, 1853–1867, 2008.
- 685 Pozzer, A., Zimmermann, P., Doering, U. M., van Aardenne, J., Tost, H., Dentener, F., Janssens-Maenhout, G.,
686 and Lelieveld, J.: Effects of business-as-usual anthropogenic emissions on air quality, *Atmos. Chem. Phys.*, 12,
687 6915–6937, doi:10.5194/acp-12-6915-2012, 2012.
- 688 Purkait, N. N., De, S., Sen, S., and Chakrabarty, D. K.: Surface ozone and its precursors at its two sites in the
689 northeast coast of India, *Indian Journal of Radio and Space Physics*, 38, 86–97, 2009.
- 690 Reddy, B. S. K., Kumar, K. R., Balakrishnaiah, G., Gopal, K. R., Reddy, R. R., Ahammed, Y. N., Narasimhulu,
691 K., Reddy, L. S. S., and Lal, S.: Observational studies on the variations in surface ozone concentration at
692 Anantapur in southern India, *Atmos. Res.* 98, 125–139, 2010.
- 693 Renuka, K., Gadhavi, H., Jayaraman, A., Lal, S., Naja, M., and Rao, S.: Study of Ozone and NO₂ over Gadanki –
694 a rural site in South India, *J. Atmos. Chem.*, 71, 95–112, doi:10.1007/s10874-014-9284-y, 2014.
- 695 Sarangi, T., Naja, M., Ojha, N., Kumar, R., Lal, S., Venkataramani, S., Kumar, A., Sagar, R., and Chandola, H. C.:
696 First simultaneous measurements of ozone, CO and NO_y at a high altitude regional representative site in the
697 central Himalayas, *J. Geophys. Res.-Atmos.*, 119, 1592–1611, doi:10.1002/2013JD020631, 2014.
- 698 Sarkar, S., Srivastava, R. K., and Sagar, K.: Diurnal Monitoring Of Surface Ozone And PM_{2.5} Concentration
699 And Its Correlation With Temperature, *INTERNATIONAL JOURNAL OF TECHNOLOGY ENHANCEMENTS*
700 *AND EMERGING ENGINEERING RESEARCH*, VOL 3, ISSUE 09, ISSN 2347-4289, 2015.
- 701 Schell, B., Ackermann, I. J., Hass, H., Binkowski, F. S., and Ebel, A.: Modeling the formation of secondary
702 organic aerosol within a comprehensive air quality model system, *J. Geophys. Res.-Atmos.*, 106, 28275–28293,
703 doi:10.1029/2001JD000384, 2001.
- 704 Sinha, V., Kumar, V., and Sarkar, C.: Chemical composition of pre-monsoon air in the Indo-Gangetic Plain
705 measured using a new PTR-MS and air quality facility: high surface ozone and strong influence of biomass
706 burning, *Atmos. Chem. Phys.*, 14, 5921–5941, 2014.
- 707 Stauffer, D. R., and Seaman, N. L.: Use of four-dimensional data assimilation in a limited area mesoscale model.
708 Part I: Experiments with synoptic-scale data, *Monthly Weather Review* 118, 1250–1277, 1990.



- 709 Stauffer, D. R., Seaman, N. L. and Binkowski, F. S.: Use of four-dimensional data assimilation in a limited-area
710 mesoscale model. Part II: Effects of data assimilation within the planetary boundary layer, *Monthly Weather*
711 *Review* 119, 734-754, 1991.
- 712 Stockwell, W. R., Middleton, P., Chang, J. S., and Tang, X.: The second generation regional Acid Deposition
713 Model chemical mechanism for regional air quality modeling, *J. Geophys. Res.*, 95, 16343-16367, 1990.
- 714 Taylor, K. E.: Summarizing multiple aspects of model performance in a single diagram, *J. Geophys. Res.* 106:
715 7183–7192, 2001.
- 716 Tewari, M., Chen, F., Wang, W., Dudhia, J., Lemone, M. A., Mitchell, K. E., Ek, M., Gayno, G., Wegiel, J. W.
717 and Cuenca, R.: Implementation and verification of the unified Noah land-surface model in the WRF model, 20th
718 Conference on Weather Analysis and Forecasting/16th Conference on Numerical Weather Prediction, Seattle,
719 WA, American Meteorological Society, 2004.
- 720 Wiedinmyer, C., Akagi, S. K., Yokelson, R. J., Emmons, L. K., Al-Saadi, J. A., Orlando, J. J., and Soja, A. J.: The
721 Fire INventory from NCAR (FINN): a high resolution global model to estimate the emissions from open burning,
722 *Geosci. Model Dev.*, 4, 625–641, doi:10.5194/gmd-4-625-2011, 2011.
- 723 Wild, O., Zhu, X. and Prather, M. J.: Fast-J: Accurate simulation of in- and below cloud photolysis in tropospheric
724 chemical models, *Journal of Atmospheric Chemistry*, 37, 245-282, 2000.
- 725 Wilkinson, S., Mills, G., Illidge, R., and Davies, W. J.: How is ozone pollution reducing our food supply?, *J. Exp.*
726 *Bot.*, 63, 527–536, doi:10.1093/jxb/err317, 2012.
- 727 Yadav, R., Sahu, L. K., Jaaffrey, S. N. A., and Beig, G.: Distributions of ozone and related trace gases at an urban
728 site in western India. *J. Atmos. Chem.* 71, 125–144, 2014.
- 729 Yoon, J. and Pozzer, A.: Model-simulated trend of surface carbon monoxide for the 2001–2010 decade, *Atmos.*
730 *Chem. Phys.*, 14, 10465-10482, doi:10.5194/acp-14-10465-2014, 2014.
- 731 Zanis, P., Hadjinicolaou, P., Pozzer, A., Tyrllis, E., Dafka, S., Mihalopoulos, N., and Lelieveld, J.: Summertime
732 free-tropospheric ozone pool over the eastern Mediterranean/Middle East, *Atmos. Chem. Phys.*, 14, 115-132,
733 doi:10.5194/acp-14-115-2014, 2014.
- 734 Zhang, Q., Streets, D. G., Carmichael, G. R., He, K. B., Huo, H., Kannari, A., Klimont, Z., Park, I. S., Reddy, S.,
735 Fu, J. S., Chen, D., Duan, L., Lei, Y., Wang, L. T., and Yao, Z. L.: Asian emissions in 2006 for the NASA
736 INTEX-B mission, *Atmos. Chem. Phys.*, 9, 5131–5153, doi:10.5194/acp-9-5131-2009, 2009.
- 737
- 738
- 739
- 740



741 **Table 1.** Abbreviations/ Acronym

EDGAR	Emission Database for Global Atmospheric Research
HTAP	Hemispheric Transport of Air Pollution
IGP	Indo Gangetic plain
IST	Indian standard time
INTEX-B	Intercontinental Chemical Transport Experiment Phase B
MB	Mean Bias
MOZART	Model for Ozone and Related Chemical Tracers
NMB	Normalized mean bias
PBL	Planetary boundary layer
RMSD	Centered root mean squared difference
RRTM	Rapid Radiative Transfer Model
SEAC4RS	Southeast Asia Composition, Cloud, Climate Coupling Regional Study
WRF-Chem	Weather research and forecasting model coupled with chemistry

742

743

744 **Table 2.** Sub-regional estimates of anthropogenic emissions (in million mol h⁻¹) in the three emission inventories
 745 used

Region	HTAP			INTEX-B			SEAC4RS		
	NO _x	NMVOC	CO	NO _x	NMVOC	CO	NO _x	NMVOC	CO
North	8.1	14.0	110.0	6.3	10.0	96.1	8.7	10.7	86.9
East	5.8	10.1	102.9	6.0	6.9	78.8	6.7	8.2	72.4
West	2.9	4.6	31.0	1.8	2.1	24.7	3.7	2.9	24.3
Central	4.6	4.2	44.6	2.0	2.9	34.7	4.9	3.1	26.2
South	5.4	5.8	37.2	2.7	4.1	46.2	3.5	3.4	28.3
Total	26.8	38.7	325.7	18.8	26.0	280.5	27.5	28.3	238

746

747

748 **Table 3.** A brief description of the different WRF-Chem simulations conducted

Sr. No.	Simulation name	Emission Inventory	Year of Emission Inventory	Spatial Resolution of Emission Inventory	Chemical Mechanism
1	HTAP-RADM2	HTAP	2010	0.1°x 0.1°	RADM2
2	INTEX-RADM2	INTEX-B	2006	0.5°x 0.5°	RADM2
3	S4RS-RADM2	SEAC4RS	2012	0.1°x 0.1°	RADM2
4	HTAP-MOZ	HTAP	2010	0.1°x 0.1°	MOZART-4

749

750

751

752

753

754

755

756



757 **Table 4.** List of observation sites and data sources used. Site nomenclature in brackets in column 1 is used in
 758 figures 1, 5, 6, 9 and 10.
 759

Site	Type	Latitude	Longitude	Altitude (m.a.s.l)	Data period	Reference
Mohali (MOH)	Urban	30.7°N	76.7°E	310	May 2012	Sinha et al. (2014)
Nainital (NTL)	Highly complex	29.37°N	79.45°E	1958	Apr 2011	Saranghi et al. (2014)
Pantnagar (PNT)	Urban/complex	29.0°N	79.5°E	231	Apr 2009-11	Ojha et al. (2012)
Delhi (DEL)	Urban	28.65°N	77.27°E	220	Apr 2013	SAFAR data
Dibrugarh (DBG)	Rural/complex	27.4°N	94.9°E	111	Apr 2010-13	Bhuyan et al. (2014)
Darjeeling*	Complex	27.01°N	88.25°E	2134	Apr 2004	Lal (2007)
Kanpur (KNP)	Urban	26.46°N	80.33°E	125	Mar-May 2010-13	Gaur et al. (2014)
Mt. Abu (ABU)	Highly complex	24.6°N	72.7°E	1680	Apr 1993-2000	Naja et al. (2003)
Udaipur (UDP)	Urban	24.58°N	73.68°E	598	Apr 2010	Yadav et al. (2014)
Jabalpur (JBL)	Complex	23.17°N	79.92°E	411	Apr 2013	Sarkar et al. (2015)
Ahmedabad (ABD)	Urban	23.03°N	72.58°E	53	May 2011	Mallik et al. (2015)
Haldia (HAL)	Urban/coastal	22.05°N	88.03°E	8	Apr 2004	Purkait et al. (2009)
Bhubaneswar (BBR)	Urban	21.25°N	85.25°E	45	Mar-May 2010	Mahapatra et al. (2012)
Johrapur (JHP)	Rural	19.3°N	75.2°E	474	Apr 2002-2004	Debaje et al. (2006)
Pune (PUN)	Urban	18.54°N	73.81°E	559	Mar-May 2013	SAFAR data
Anantapur (ANP)	Rural	14.62°N	77.65°E	331	Apr 2009	Reddy et al. (2010)
Gadanki (GDK)	Rural	13.48°N	79.18°E	375	Mar-May 2010-11	Renuka et al. (2014)
Kannur (KNR)	Rural/coastal	11.9°N	75.4°E	5	Apr 2010	Nishanth et al. (2012)
Thumba/Trivendrum (TRI)	Urban/coastal	8.55°N	77°E	3	Apr 2009	David et al. (2011)

760
 761 * At Darjeeling only monthly mean value is available.
 762
 763

764 **Table 5.** A comparison of correlation coefficients (r) over different regions for the four simulations

Region	HTAP-RADM2	INTEX-RADM2	S4RS-RADM2	HTAP-MOZ
North	0.90	0.86	0.88	0.90
East	0.98	0.97	0.97	0.98
West	0.99	0.98	0.98	0.99
Central	0.70	0.67	0.69	0.75
South	0.99	0.98	0.97	0.97
Overall	0.98	0.97	0.97	0.99

765
 766
 767



768 **Table 6.** A comparison of noontime (1130-1630 IST) average mean biases in ppbv over different regions for the
 769 four simulations

Region	HTAP-RADM2	INTEX-RADM2	S4RS-RADM2	HTAP-MOZ
North	2.4	-3.3	-4.1	8.3
East	19.5	19.5	15.3	29.9
West	11.4	8.0	9.0	14.0
Central	0.9	-8.0	-2.5	8.8
South	15.3	8.2	6.5	25.5
Overall	10.5	5.9	5.2	17.3

770

771

772

773

774 **Table 7.** Recommendations based on noontime average mean biases over different regions for the four
 775 simulations

Region	HTAP-RADM2	INTEX-RADM2	S4RS-RADM2	HTAP-MOZ
North	√			
East			√	
West		√		
Central	√			
South			√	
Overall			√	

776

777

778

779

780

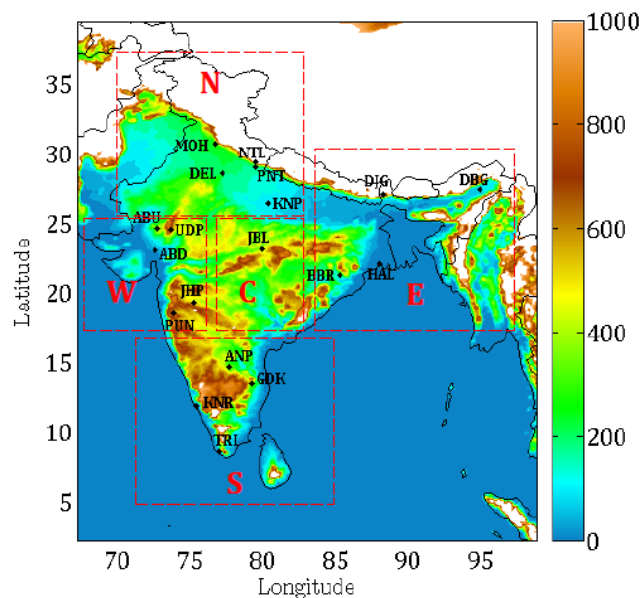
781

782

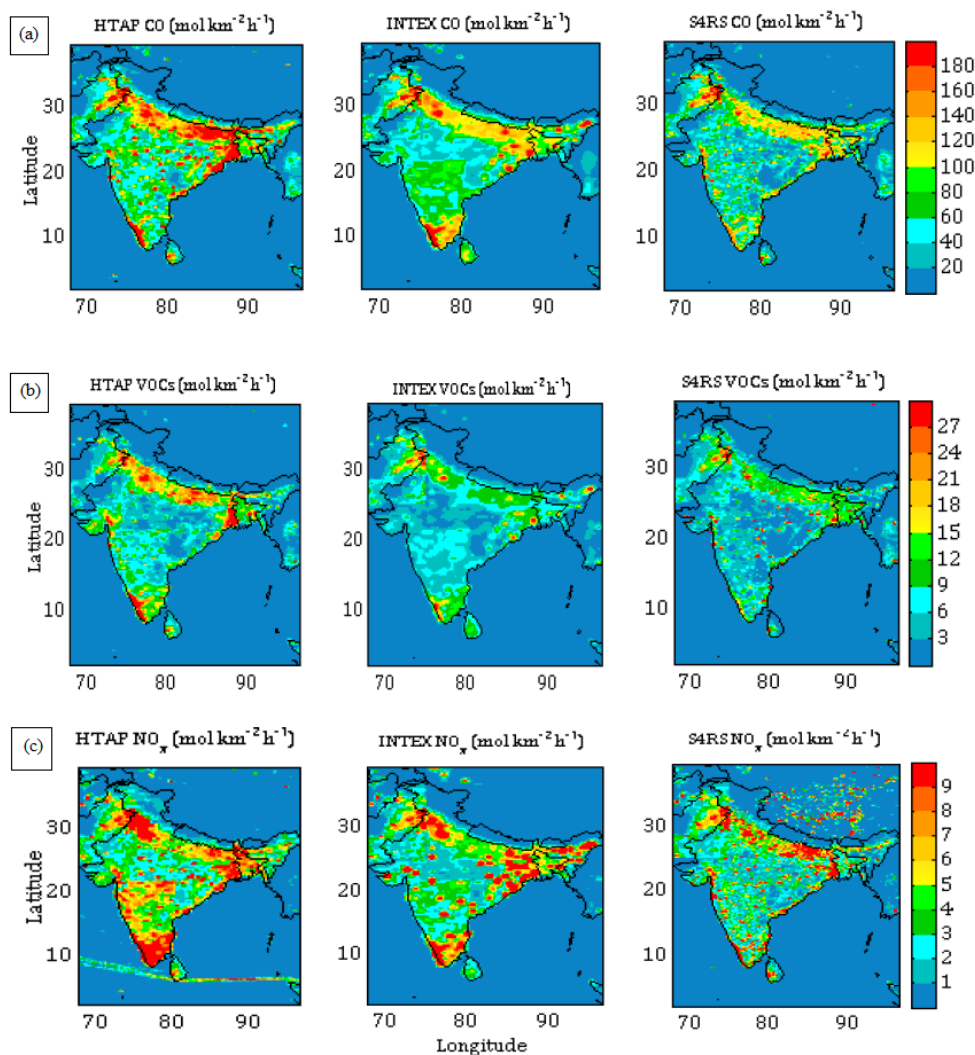
783

784

785



786
787 **Figure 1.** Simulation domain showing terrain height (in metres) and observation sites. White region indicates that the terrain
788 height is equal to or exceeds 1 km. The domain is subdivided into five regions viz. North (N), South (S), East (E), West (W)
789 and central (C) regions, as shown by red rectangles.
790
791
792
793
794
795
796
797
798
799
800
801
802
803
804
805



806

807 **Figure 2.** A comparison of (a) CO, (b) NMVOC and (c) NO_x emissions between the three inventories used (see Section-2.2 for
808 description).

809

810

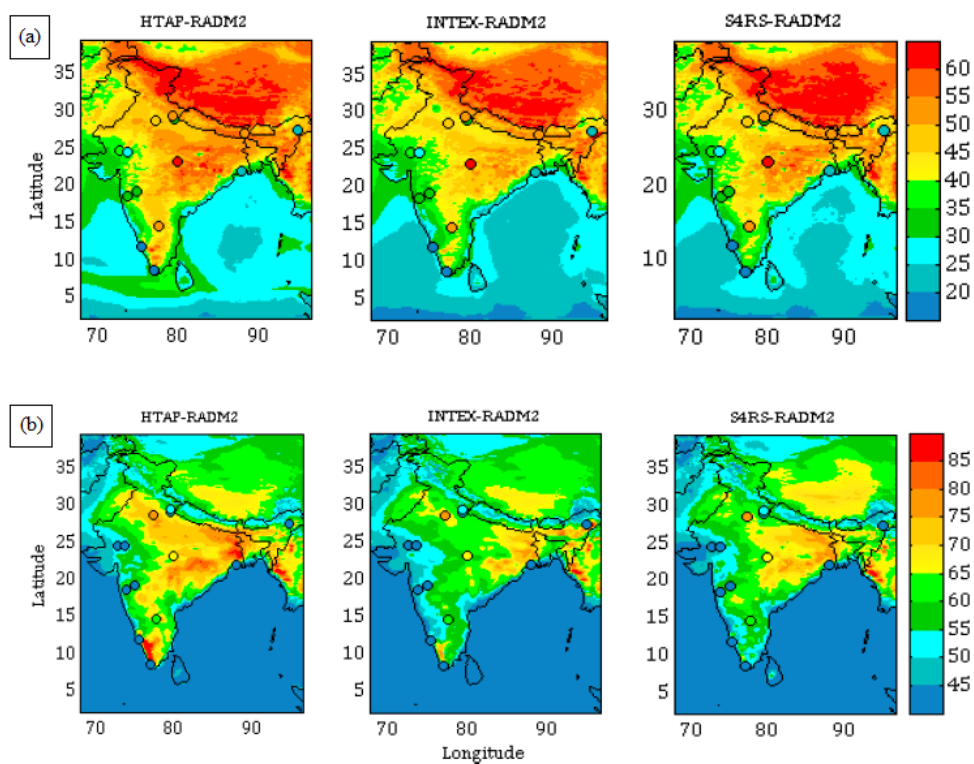
811

812

813

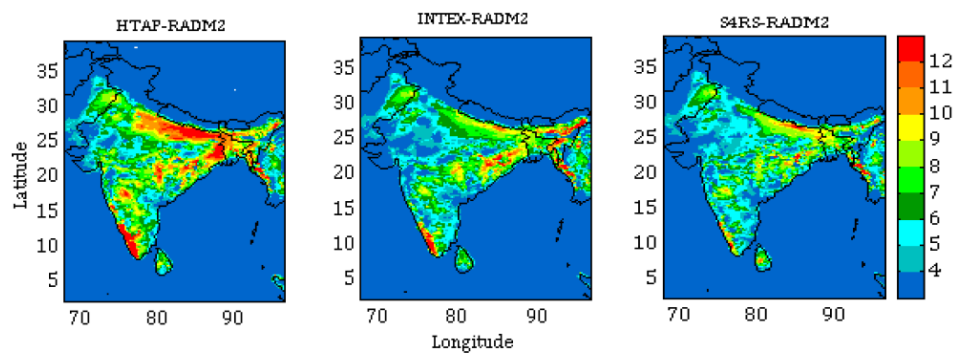
814

815



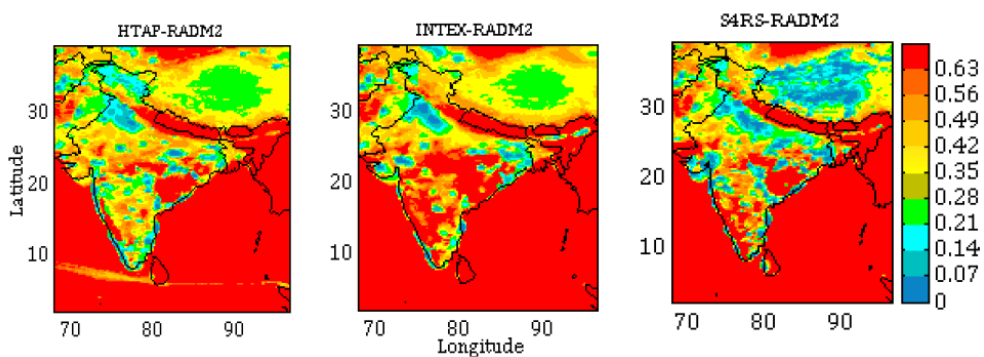
816
817 **Figure 3.** Spatial distribution of monthly (for April) average surface ozone calculated for (a) 24 h and (b) noontime (1130-1630
818 IST). The average ozone mixing ratios (ppbv) from observations are also shown for comparison on the same colour scale. Note
819 the difference in colour scales in the top and bottom rows.

820
821
822
823
824
825
826
827
828

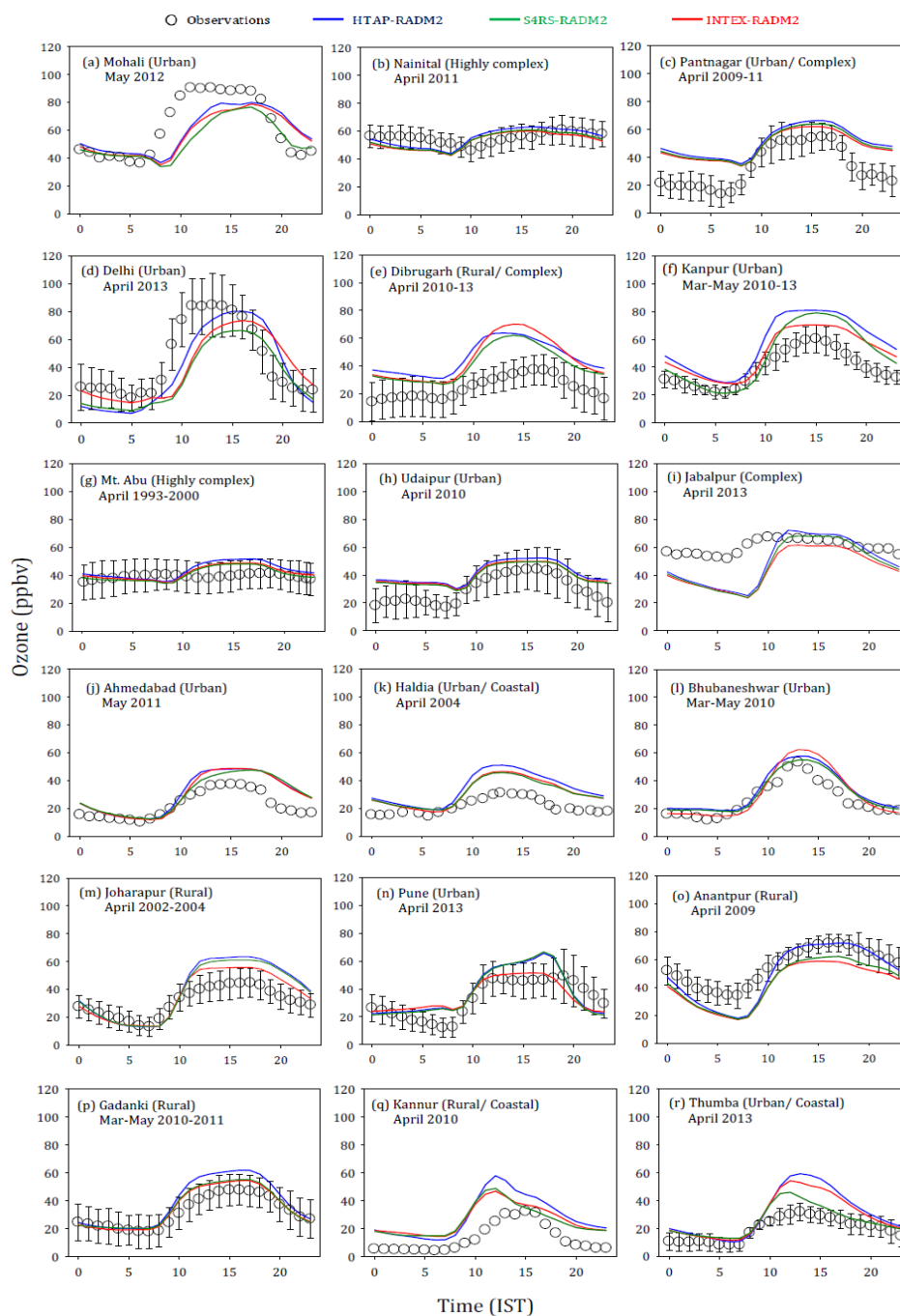


829
830 **Figure 4.** Spatial distribution of net daytime surface ozone chemical tendency (in ppbv h⁻¹) for the month April during 0630-
831 1230 IST
832

833
834
835
836
837
838
839
840
841
842
843
844
845
846
847
848
849
850
851
852
853



854
855 **Figure 5.** Spatial distribution of net daytime surface CH_2O to NO_y ratio in simulations with different inventories for the month
856 April during 0630-1230 IST
857

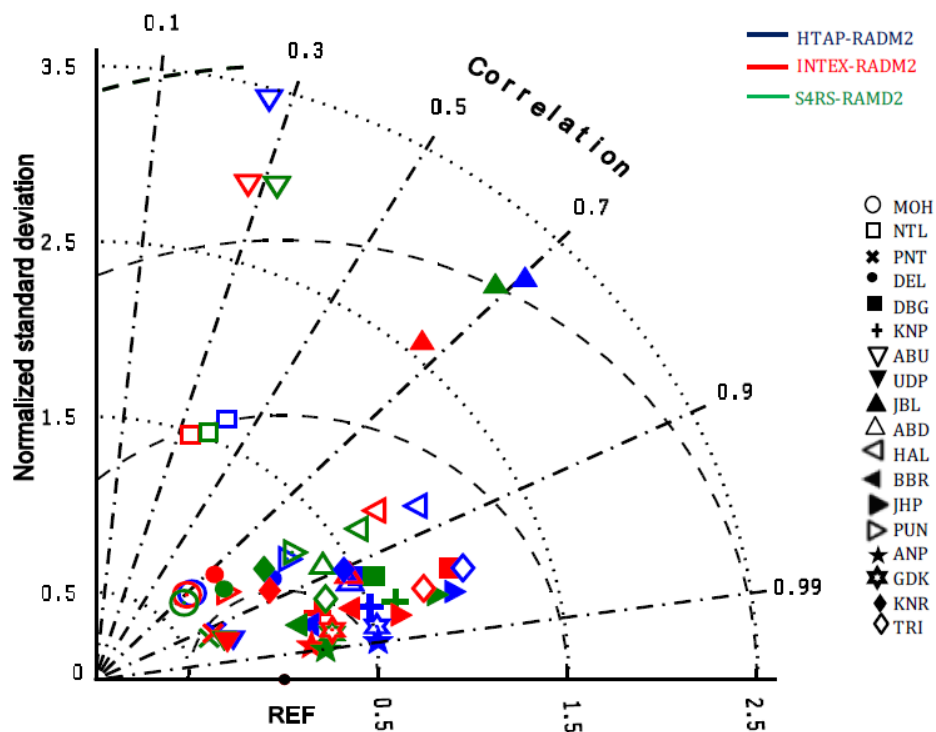


858

859 **Figure 6.** Comparison of monthly average diurnal variation of surface ozone simulated using different emission inventories at
860 various observation sites. The observational data is available for the period indicated in the figure whereas all model
861 simulations are for the year 2013. Error bars represent the temporal standard deviations of the monthly averages. All model
862 simulations are with RADM2 chemistry.



863



864

865 **Figure 7.** Taylor diagram showing model statistics (r , normalized standard deviation and RMSD) at all sites. The correlation is
866 the cosine of the angle from the horizontal axis, the root mean square difference is the distance from the reference point (REF)
867 and the standard deviation is the distance from the origin.

868

869

870

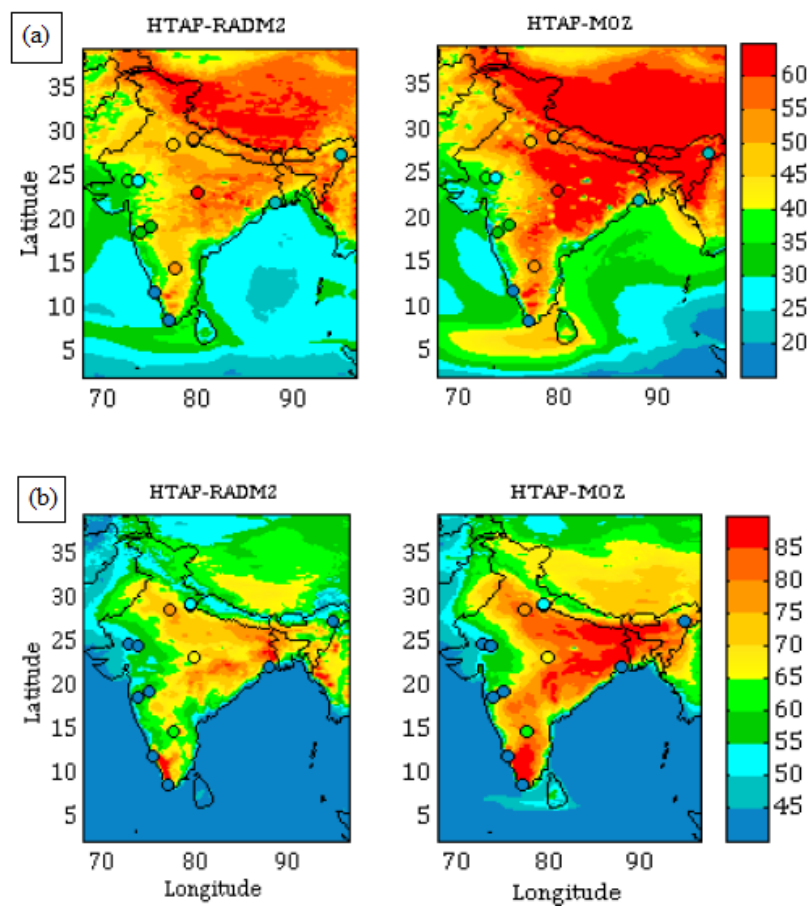
871

872

873

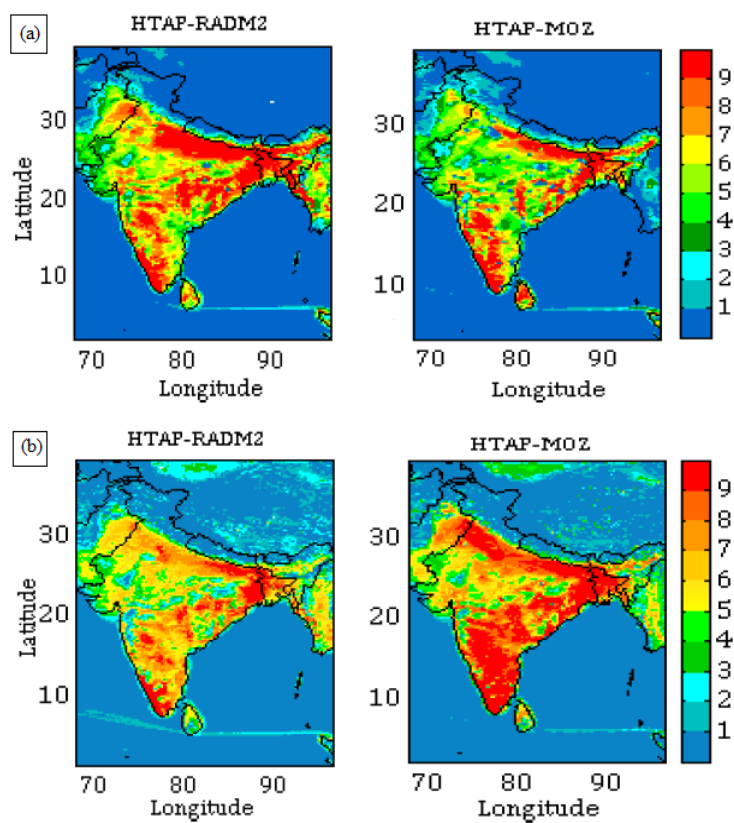
874

875



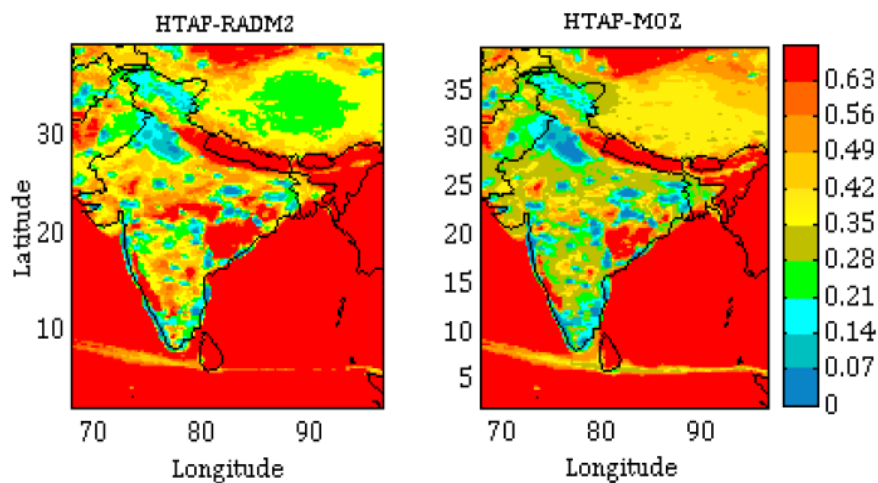
876
877 **Figure 8.** Spatial distribution of monthly (April) average surface ozone calculated for (a) 24 h and (b) noontime (1130-1630
878 IST), comparing the chemical mechanisms (RADM2 and MOZART). The average ozone mixing ratios (ppbv) from
879 observations are also shown for comparison on the same colour scale. Note the difference in colour scales in the top and bottom
880 rows.
881

882
883
884
885
886
887
888
889
890
891
892

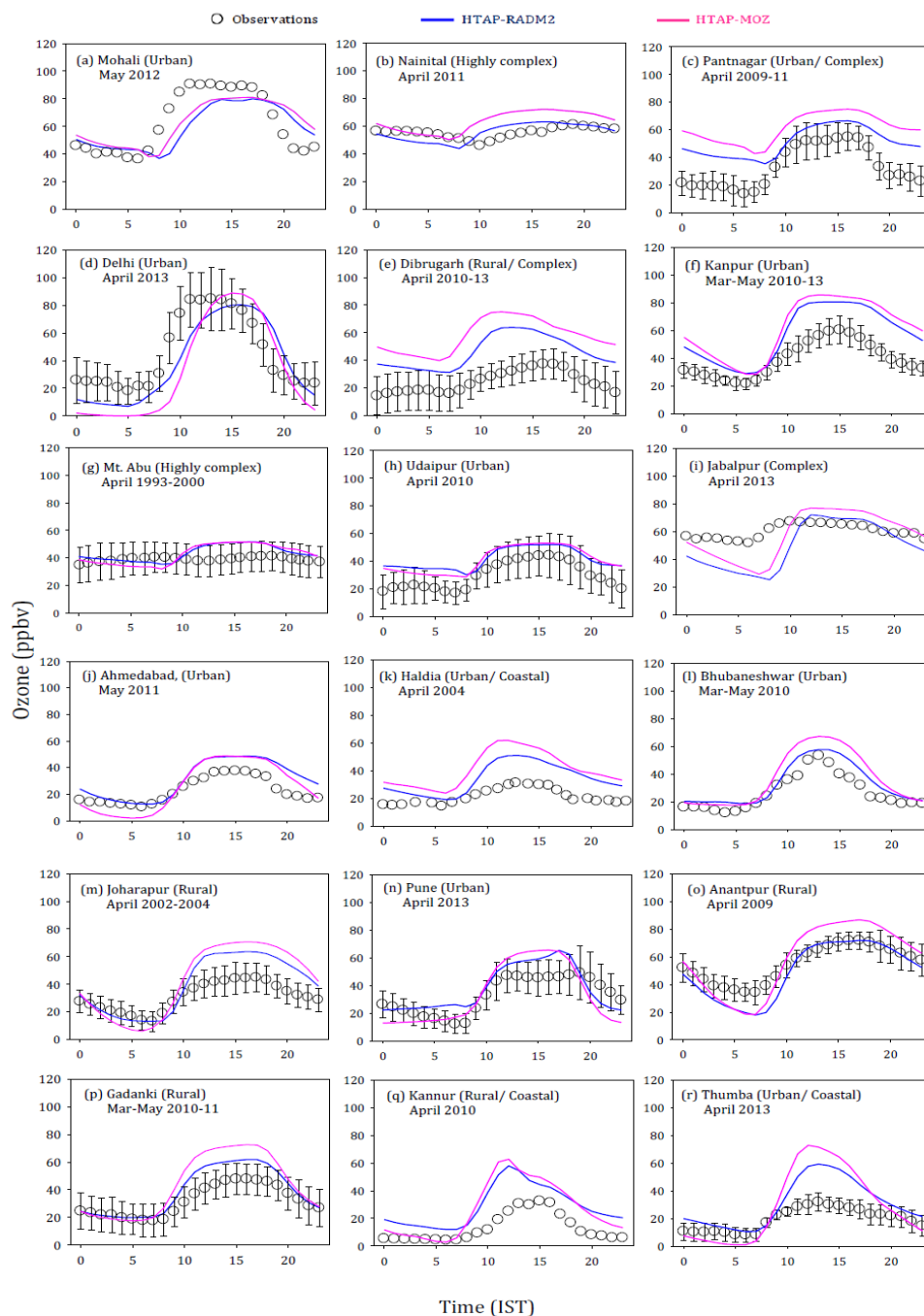


893
894 **Figure 9.** Spatial distribution of average (a) net daytime surface ozone chemical tendency (in ppbv h⁻¹) (b) net daytime surface
895 ozone chemical +vertical mixing tendency (in ppbv h⁻¹) for April during 0630-1230 IST
896

897
898
899
900
901
902
903
904
905
906
907
908
909
910
911
912

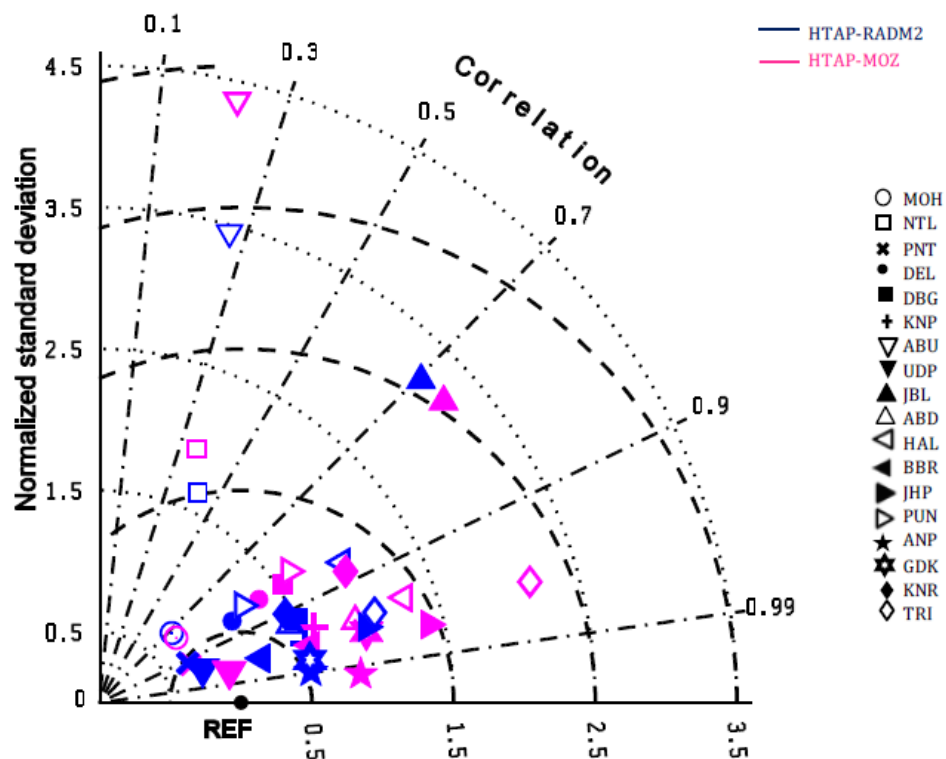


913
914 **Figure 10.** Spatial distribution of net daytime surface CH_2O to NO_y ratio in simulations with different chemical mechanisms
915 for the month April during 0630-1230 IST
916



917

918 **Figure 11.** Comparison of monthly average diurnal variation of surface ozone simulated using different chemical mechanisms
919 at various observation sites. The observational data is available for the period indicated in the figure whereas all the model
920 simulations are for the year 2013. Error bars represent the temporal standard deviations of the monthly averages. All model
921 simulations are with HTAP inventory.



922

923 **Figure 12.** Taylor diagram showing model statistics (r , normalized standard deviation and RMSD) at all sites. The correlation is
 924 the cosine of the angle from the horizontal axis, the root mean square difference is the distance from the reference point (REF)
 925 and the standard deviation is the distance from the origin.

926

927

928

929

930

931

932

933

934

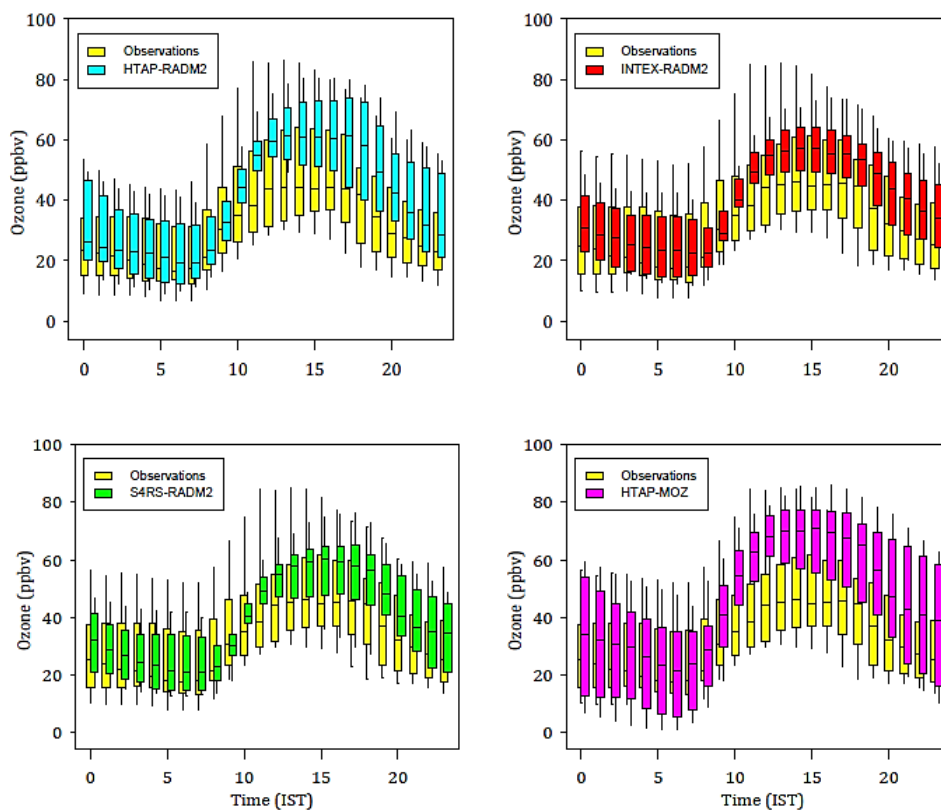
935

936

937



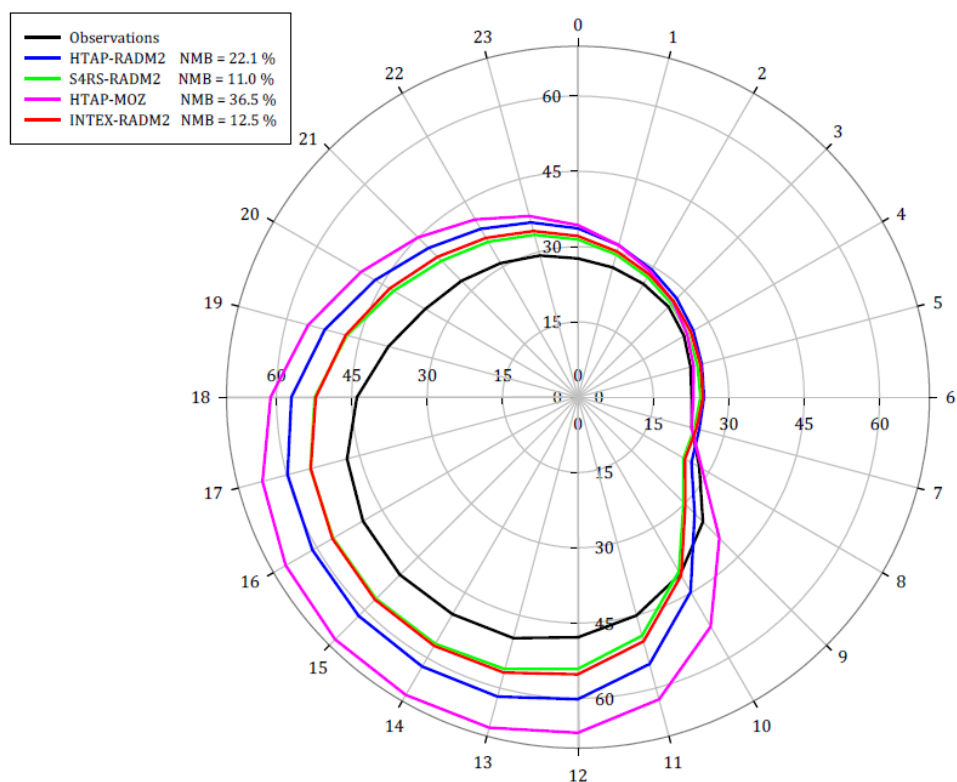
938



939
940

941 **Figure 13.** A box/whisker plot comparison of monthly average diurnal variation of surface ozone from model runs and
942 observations over the entire domain (after spatially averaging the results). Upper and lower boundaries of boxes denote the
943 75th and 25th percentiles and whiskers represent the 95th and 5th percentiles. The line inside the box is the median.

944
945
946
947
948
949
950
951
952
953
954
955
956



957
958
959
960
961
962

Figure 14. Polar plot for monthly mean diurnal variation of surface ozone (in ppbv) from all model simulations and observations each spatially averaged over all sites. The numbers on the outermost circle represent the hour of the day and the radial distance from the centre represents surface ozone mixing ratios in ppbv. The normalized mean bias (NMB in %) values in all the simulations are also provided in the caption box.